Reduced amphibolite facies conditions in the Precambrian continental crust of the Siberian craton recorded by mafic granulite xenoliths from the Udachnaya kimberlite pipe, Yakutia

A.L. Perchuk [a,b,*], A.V. Sapegina [a,b], O.G. Safonov [a,b,c], V.O. Yapaskurt [a], V.S. Shatsky [d], V. G. Malkovets [d,e]

[a] Department of Petrology and Volcanology, Geological Faculty, Moscow State University, Moscow, Russia
[b] Korzhinskii Institute of Experimental Mineralogy, Russian Academy of Sciences, Chernogolovka, Russia
[c] Department of Geology, University of Johannesburg, Johannesburg, South Africa
[d] Sobolev Institute of Geology and Mineralogy, Siberian Branch of Russian Academy of Sciences, Novosibirsk, Russia
[e] ALROSA Geological Research Enterprise (Public Joint-Stock Company), Chernyshevskoe Shosse 16, Mirnyi, Russia

ARTICLE INFO

ABSTRACT

It is widely accepted that granulite xenoliths from kimberlites provide a record of granulite facies metamorphism at the basement of cratons worldwide. However, application of the phase equilibria modeling for seven representative samples of mafic granulites from xenoliths of the Udachnaya kimberlite pipe, Yakutia, revealed that a granulitic garnet + clinopyroxene + plagioclase ± orthopyroxene ± amphibole ± scapolite mineral assemblage was likely formed in the middle crust under amphibolite facies conditions (600–650 °C and 0.8–1.0 GPa) in a deficiency of fluid. Clinopyroxene in the rocks is characterized by elevated aegirine content (up to 10 mol.%) both in the earlier magmatic cores and in the later metamorphic rim zones of the grains. Nevertheless, the phase equilibrium modeling for all samples indicates surprisingly reduced conditions, i.e. oxygen fugacity 1.6–3.3 log units below the FMQ (Fayalite-Magnetite-Quartz) buffer. In contrast, the coexistence of Fe-Ti oxides indicates temperatures of 850–990 °C and oxygen fugacity about lg(FMQ) ± 0.5, conditions which correspond to earlier stages of rock evolution. Reduction of oxygen fugacity during cooling is discussed in the context of the evolution of a complex fluid. The reconstructed P-T conditions for the final equilibration in the mafic granulites indicate that temperatures were ~250 °C higher than those extrapolated from the continental conductive geotherm of 35–40 µW/m² deduced from peridotite xenoliths of the Udachnaya pipe. Although the granulites resided in the crust for a period for at least 1.4 Ga, they did not re-equilibrate to the temperatures of the geotherm, likely due to the blocking of mineral reactions under relatively low temperatures and fluid-deficient conditions

1. Introduction

The oldest continental crust is stored in the Archean and Paleoproteroic cratons, which represent large, coherent cores of ancient continents underlain by an anomalously thick, light (melt-depleted), and cold subcratonic lithospheric mantle. A significant portion of the upper and middle continental crust is composed of voluminous tonalite-trondjemite-granodiorite (TTG) granitoids and gneisses, the origin of which (subduction vs. mantle plume regimes) remains debatable (Condie and Abbott, 1999; Van Kranendonk, 2010; Moyen and Martin, 2012; Arndt, 2013; Cawood et al., 2013; Rozel et al., 2017). The lower crust is composed predominantly of metabasic rocks (granulites and, to a lesser

extent, amphibolites), which are often related to the metamorphic modification of rocks crystallized from mafic magmas derived from the upwelling mantle (Bohlen and Mezger, 1989; Rudnick, 1995; Rudnick and Fountain, 1995; Gao et al., 2004; Shatsky et al., 2018). As an alternative, mafic rocks can also be incorporated into the middle-lower crust via gravitational sinking or 'sagduction' of the overlying material of greenstone belts and opposite diapiric rise of gneisses and granitic plutons (Anhaeusser, 1975; Van Kranendonk, 2004; Perchuk et al., 2011, 2018; Thébaud and Rey, 2013; François et al., 2014; Johnson et al., 2016; Brown and Johnson, 2018).

Suites of the lower crustal xenoliths from different kimberlite localities worldwide provide a wide range of metamorphic temperatures

---

(650–1000 °C) (e.g. Rudnick, 1992). These temperatures are lower for the xenolith from "on-craton" kimberlites than from "off-craton" ones (e. g. Pearson et al. 1995). Notably, a similar tendency is documented for the underlying mantle, i.e. subcratonic mantle is colder than off-cratonic mantle (Griffin et al., 2003; Goncharov and Ionov, 2012). However, temperatures recorded by the lower crustal rocks are notably above the paleogeotherms deduced from the corresponding mantle peridotite xenoliths (Rudnick, 1992; Pearson et al., 1995). This inconsistency is usually explained by the blocking temperature of cation exchange reactions that have not been reset during cooling of the rocks (e.g. Rudnick, 1992).

Granulite xenoliths usually provide no record of their P-T evolution. However, rare studies show sub-isobaric cooling P-T paths at the lower crustal depths (e.g. Pearson et al., 1995). Such P-T evolution is consistent with the hypothesis of crustal thickening by crystallization of mafic magmas near the crust-mantle boundary (Bohlen and Mezger, 1989).

The Udachnaya kimberlite pipe (Yakutia) is a treasury of fresh xenoliths transported from different levels of the crust and, thus, represents an excellent testing ground for studies of formation and evolution of the Siberian craton. Granulite xenoliths were the focus of previous studies (Shatsky et al., 1990, 2005, 2016, 2019; Koreshkova et al., 2009; Koreshkova et al., 2011; Moyen et al., 2017). These studies revealed magmatic protolith, the timing of two major tectono-thermal events, and a wide range of P-T metamorphic conditions. Despite intensive study, oxygen fugacity (f_{O2}) has never been evaluated for these rocks or for crustal xenoliths worldwide. P-T parameters for xenoliths were obtained exclusively using conventional mineral thermobarometry. The method of phase equilibria modeling (Powell et al., 1998; Connolly, 2005), which is widely applied to reconstruct metamorphic conditions of mafic granulites from orogenic belts (e.g. Yang and Wei, 2017; Kunz and White, 2019), had never been applied to crustal xenoliths.

In the present study, we report results of a detailed petrologic study of representative mafic granulite xenolith samples from the Udachnaya kimberlite pipe that shows revised P-T conditions and specifies f_{O2} deciphered using the method of phase equilibrium modeling (PERPLE_X software; Connolly, 2005).

2. Geological setting

The basement of the Siberian Craton is subdivided into four major tectonic provinces: the Anabar in the center, the Olenek in the northeast, the Tungus in the west, and the Aldan in the southeast (Pisarevsky et al., 2008; Rosen et al., 1994, 2006) (Fig. 1). The Anabar tectonic province is separated from the Aldan province by the Proterozoic Akitkan fold belt, from the Tungus province by the north-striking Sayano-Taymyr suture zone, and from the Olenek province by the northwest-striking Bilyakh suture zone. Much of the Siberian craton is under 2–14 km-thick sedimentary cover and voluminous Triassic flood basalts (Siberian traps). The total thickness of the continental crust of the craton is 40–45 km (Suvorov et al., 2006; Koreshkova et al., 2011). According to Rosen et al. (2006), the Siberian craton was finally formed in the Paleoproterozoic (2.0–1.8 Ga) due to the assembly of the Daldyn, Marha, and Magan terranes; this process is probably recorded by zircon ages in mafic xenoliths (Fig. 1, inset).

Kimberlite pipes occur in the Olenek and Anabar provinces only. The latter province contains six kimberlite fields (Fig. 1). Kimberlite magmatism on the Siberian Craton occurred in four distinct episodes: Silurian–Early Devonian (~420–400 My), Late Devonian (~360 My), Triassic (~235 My), and Jurassic (~150 My) (Tretiakova et al., 2017 and references therein). Diamond-rich kimberlites are overwhelmingly Late Devonian (~360 My) in age. The Udachnaya diamondiferous kimberlite pipe is located in the Daldyn kimberlite field of the Daldyn terrane; it intruded into sedimentary cover in the Devonian (Kinny et al., 1997). The kimberlite pipe bears a large variety of mantle and crustal xenoliths hosted by exceptionally fresh kimberlites (e.g., Boyd et al., 1997; Kamenetsky et al., 2007). Mantle xenoliths are represented by
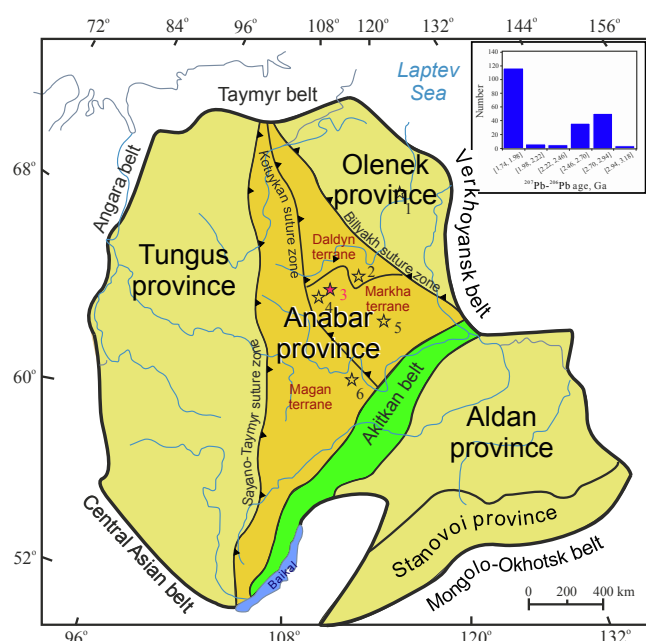

Fig. 1. Simplified geological scheme of the Siberian craton (modified after Rosen et al., 2006; Shatsky et al., 2016, 2019). Heavy solid lines delineate boundaries of the Siberian craton; solid lines indicate boundaries between its major units which are indicated by different colors. Stars indicate kimberlite fields: 1 – Kuoyka field (Obnazhennaya pipe); 2 – Muna field (Novinka and Zapolyarnaya pipes); 3 (red star) – Daldyn field (Udachnaya, Leningradskaya and Zarnitsa pipes); 4 – Alakit field (Komsomolskaya pipe); 5. Nakyn field (Nyurbinskaya, Botuobinskaya pipes); 6 – Kharamai kimberlite field. The inset: a histogram summarizing U-Pb SHRIMP ages of zircons from mafic xenoliths from the Udachnaya kimberlite pipe (Koreshkova et al., 2009; Shatsky et al., 2016, 2018; Moyen et al., 2017).

eclogites and peridotites (Doucet et al., 2014; Goncharov et al., 2012; Agashev et al., 2013; Shatsky et al., 2008, 2016; Liu et al., 2009), lower crustal xenoliths by mafic granulites, amphibolites, plagiogneisses, and metapelites (Shatsky et al., 1990, 2005; 2018; Koreshkova et al., 2011; Ionov et al., 2015; Moyen et al., 2017), and upper crustal xenoliths by tonalites and granites (Moyen et al., 2017).

The mafic xenoliths are composed of the garnet + clinopyroxene + plagioclase ± othopyroxene ± amphibole ± scapolite mineral assemblage. They show the Archean Hf model zircon ages of $T_{DM} = 3.13–2.5$ Ga and provide evidence for at least two tectonothermal events recorded by U-Pb isotope systematics in zircon: Neoarchean (2.9–2.7 Ga) and Paleoproterozoic (2.0–1.8 Ga) (inset in Fig. 1). Based on the geochemistry of crustal and mantle xenoliths from the Udachnaya kimberlite pipe, Moyen et al. (2017) proposed that the upper crust of the Siberian Craton was formed in the Archean (ca. 2.7 Ga), while the lower crust and lithospheric mantle experienced either a complete or a large-scale delamination and rejuvenation in the Paleoproterozoic (~1.8 Ga). However, using a compilation of isotopic and geochemical data on crustal rocks and SCLM peridotites, Shatsky et al. (2019) argued that the model by Moyen et al. (2017) is valid only for the local section under the Udachnaya pipe. The rest of the Anabar tectonic province crust (Fig. 1) is composed of variably reworked Paleoarchean rocks and juvenile Proterozoic rocks situated at different crustal levels. According to Shatsky et al. (2016), Shatsky et al. (2018), Shatsky et al. (2019), the crust of the Siberian Craton was coupled with subcratonic lithospheric mantle since the Paleoarchean.

3. Analytical methods

Analyses of minerals were performed using the Jeol 6480 LV SEM equipped with the INCA – Energy 350 EDS detector and the INCA Wave

500 WDS detector (Oxford instruments) at the Laboratory of Local Methods of Analysis at the Department of Petrology and Volcanology, Moscow State University Geological Faculty. Analytical conditions for the analyses were 15 kV acceleration voltage, 15nA beam current, and counting times of 100 s. The ZAF matrix correction was applied.

The JXA-8230 Jeol Superprobe at the same laboratory was used to analyze both major and some trace elements (Ti, Sc, Y, P, Cr) in garnet. The analytical conditions for the Superprobe analyses were 20 kV acceleration voltage and 60 nA beam current. Counting times for major elements were similar for both the standards and the sample: 40 s for Mg, Ca, and Fe, and 20 s for Al and Si. The dispersion of the measured concentration during the major element analyses using the above conditions did not exceed 0.5%. The following crystalline standards were used for the minor element analyses: $MnTiO_3$ for Ti-$K\alpha_1$ and Mn-$K\alpha_1$; Cr_2O_3 for Cr-$K\alpha_1$; $ScPO_4$ for P-$K\alpha_1$ and Sc-$K\alpha_1$; and $Y_3Al_5O_{12}$ for Y-$L\alpha_1$. The Ti, Mn, Cr measurements (crystal LiF) and P measurements (crystal PET-J) were performed using spectrometers with a 140 mm radius Rowland circle, whereas Sc and Y (crystal PET-H) were measured using the 100 mm radius H-type spectrometer. The position of maxima for the trace elements in garnets was specified by means of slow scanning of the corresponding spectral intervals. Counting time was set to attain the detection limit of 0.005 wt%: 30 s for Ti and Mn, 40 s for Cr, 60 s for P and Y, and 80 s for Sc. ZAF correction was applied for analyses. Analytical conditions for the elemental mapping using the JXA-8230 Jeol Superprobe were the same as for individual spot analyses.

The proportion of ferric iron in microprobe analyses of amphiboles was calculated for 13 cations/23 oxygens (Schumacher, 1997), and in clinopyroxenes and garnets for 4 cations/6 oxygens and 8 cations/12 oxygens, respectively (Brandelik, 2009, CALCMIN program). Mole fractions of aegirine and jadeite end-members in clinopyroxenes were calculated according to the method of Lindsley (1983). Symbols of minerals are after Whitney and Evans (2010).

Qualitative identification of lamellae in clinopyroxene was performed by means of Raman spectroscopy using the JY Horiba XPloRa Jobin spectrometer equipped with a polarized Olympus BX41 microscope at the Department of Petrology and Volcanology. Spectra were obtained using a 532 nm laser within the range of 100–4000 cm^{-1} for 30 sec. The spectra were refined with LabSpec (version 5.78.24) software. Crystalline phases were identified using the rruff.info database.

4. Petrography and mineral chemistry

The mafic crustal xenoliths considered in this study were collected in the ore storage near the Udachnaya kimberlite pipe (Supplementary Fig. 1). The samples are of rounded shape from 8 to 15 cm in size. They are relatively fresh with minor alteration caused by host kimberlite. The samples are composed of the Cpx + Grt + Pl ± Opx ± Amp ± Scp mineral assemblage. Scapolite occurs only in sample OSYB-14 (Table 1). Accessory minerals are represented by ilmenite with Ti-magnetite lamellae, apatite, and Fe-Ni-Cu sulfides. Mineral assemblages and mineral modes of the studied samples are listed in Table 1.

The samples are massive, fine- to medium-grained, with granoblastic texture (Fig. 2). Rock-forming minerals are evenly distributed in the samples. The exception is sample Ud79-24, where garnet-rich and garnet-poor domains occur in a plagioclase-two-pyroxenes matrix

(Fig. 2b, e). Samples OSYB-14 and Ud79-27 contain grains of brownish-green amphibole 1–3 mm in size, which are in a textural equilibrium with the major minerals. Scapolite in sample OSYB-14 (Fig. 3c) forms anhedral grains of up to 5 mm in size evenly distributed in the rock. Kimberlite melt/fluid-related alteration is recorded by intergranular veinlets composed mostly of phlogopite, carbonates, and serpentine. The veinlets often crosscut plagioclase grains and rarely other rock-forming minerals (Fig. 3).

Microprobe analyses of minerals and their formulas are presented in Supplementary Tables 1-3.

Clinopyroxene forms light-green grains 1–2 mm in size with rare inclusions of plagioclase or orthopyroxene (in the Opx-bearing samples). Inclusions of clinopyroxene occur mainly in garnet (Fig. 3a-d) and rarely in orthopyroxene. Clinopyroxene cores often contain pyroxene ± ilmenite lamellae easily visualized both optically and in BSE (Fig. 3a, f). Raman spectroscopy of the pyroxene lamellae in samples Ud79-24 and Ud01-300 revealed that low-Ca pyroxene in the lamellae is monoclinic, which can be interpreted as pigeonite. This finding agrees with inverted pigeonite lamellae found in clinopyroxene from similar crustal xenoliths of the Udachnaya pipe (Shatsky et al., 1990). Clinopyroxene compositions vary from diopside to augite with relatively high aegirine content ($X_{Aeg} = 0.07 – 0.15$), but minor jadeite ($X_{Jd} = 0.00 – 0.03$) (Fig. 4, Supplementary Table 1).

Matrix clinopyroxenes show clear compositional zoning. Lamella-bearing cores are compositionally homogeneous, whereas rim zones 100–200 μm wide show a general tendency for an increase of MgO and a decrease of FeO, Fe_2O_3, TiO_2, and Al_2O_3 toward the margin (about 10–20% of visible grain size) (Fig. 5, Supplementary Table 1). The zoning is usually concentric with some local enrichment in MgO at contacts with garnet. An effect of the kimberlite-related veinlets on the clinopyroxene zoning was not established.

Clinopyroxene inclusions in garnet are usually lamellae-free. However, there are several inclusions with lamellae of pyroxene (without ilmenite) in the cores. Although zoning patterns of the clinopyroxene inclusions are in general similar to those of the matrix grains (Fig. 5), their compositions in each sample overlap partly (Fig. 5). In general, clinopyroxene inclusions are depleted in Al_2O_3 and have higher X_{Mg} than matrix grains (Fig. 5, Supplementary Table 1). TiO_2 content in all inclusions decreases towards the rim (contact with host garnet) and is close to the content in the rims of matrix clinopyroxenes (Supplementary Table 1). The composition of the inclusions is similar to that of the matrix clinopyroxene rim zones. None of the inclusions in the studied samples corresponds to the core composition of matrix grains.

Garnet forms pinkish subhedral grains up to 4 mm in size and often contains inclusions of clinopyroxene, opaque minerals, and rare plagioclase and amphibole (Fig. 3a-d). Orthopyroxene is the only mineral which is not included in garnet. An early stage of inclusion trapping is visible in thin sections (Fig. 3a). The composition of garnet varies from sample to sample and falls in the range of almandine-pyrope-grossular solid solution with minor content of Fe^{3+} (Fig. 6, Supplementary Table 2). Garnets in all studied samples show a weak concentric growth zoning (similar to that noted by Koreshkova et al., 2011) with a slight increase of X_{Ca} and decrease of X_{Mg} and TiO_2 in the 100–300 μm-wide rim zone (Fig. 7). Compositions of the garnet rims are slightly variable (Fig. 5). Garnet cores contain detectable amounts of Sc_2O_3 (up to 0.02 wt

Table 1
Modal mineralogy of studied granulites xenoliths from Udachnaya kimberlite pipe.

Sample	Cpx	Grt	Pl	Opx	Qz	Amp	Scp	Ilm	Rt	Sulf	Ap
OSYV9	39	25	35			<1		3		<1	<1
OSYV14	31	24	27	<1		12	5	1	<1	<1	<1
Ud79-24	34	16	40	8		<1		2		<1	
Ud79-27	43	18	37			<1		2	<1	<1	
Ud01-127	33	20	44		<1	<1		3		<1	
Ud01-300	39	29	30			<1		2	<1	<1	
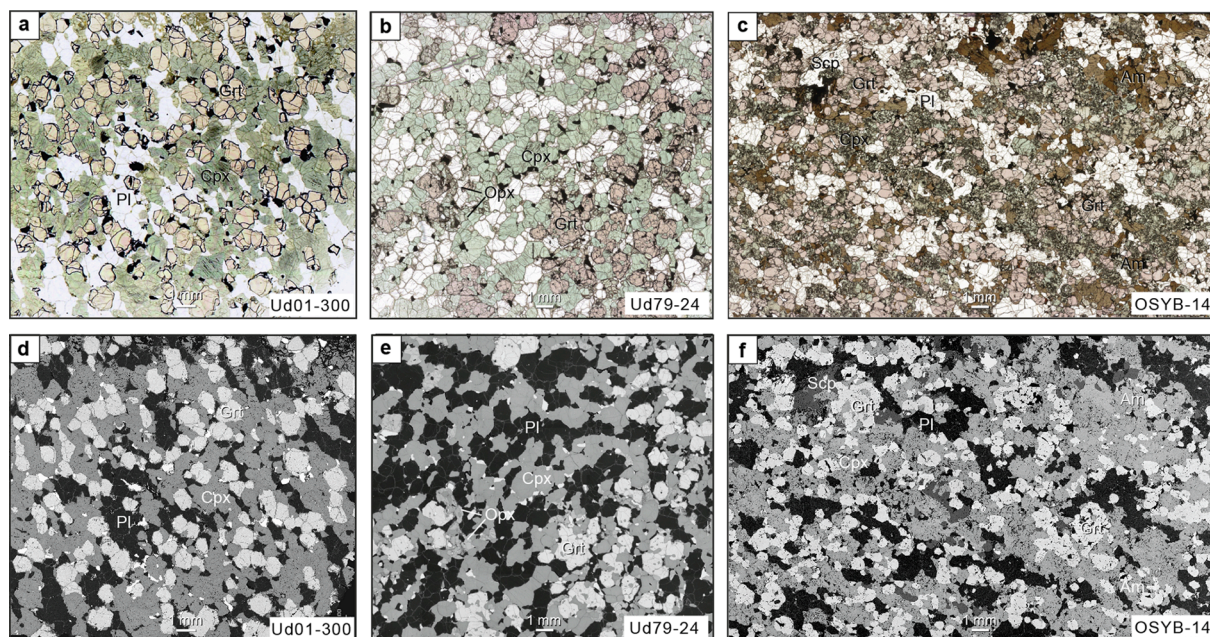
Fig. 2. General textural and structural features of the studied mafic granulite xenoliths (Ud01-300, Ud79-24, OSYB-14) with different mineral parageneses. Scan (a-c) and BSE (d-f) panoramic images of the thin sections.

%), Cr_2O_3 (up to 0.15 wt%), and P_2O_5 (up to 0.04 wt%). The concentrations of these components decrease toward the rims of garnet grains. No compositional changes of garnets caused by kimberlite melts were found.

Plagioclase forms colorless (in polarized light) subhedral grains up to 2 mm in size evenly distributed in the samples. Plagioclase composition varies from sample to sample in the range of $X_{An} = 0.25–0.48$ with the orthoclase content below 3 mol.% (Supplementary Table 3). Plagioclase grains have homogeneous cores and narrow rim zones, where the anorthite content decreases by 4–8 mol.%. Plagioclase is much more strongly affected by the kimberlite-related alteration than other minerals.

Orthopyroxene occurs as a rock-forming mineral only in sample Ud79-24. Several grains were detected in sample OSYB-14. Orthopyroxene forms elongated 0.5–1 mm grains (Fig. 3d), which tend to be located near clinopyroxene, locally trapping clinopyroxene as an inclusion. The orthopyroxene composition in both samples differs in X_{Mg} and Al_2O_3 (Fig. 8, Supplementary Table 1).

Amphibole occurs in all studied samples as mafic granulites either in a rock-forming mode (in sample OSYB-14) or as an accessory mineral (in most of the samples). It occurs mainly in the rock matrix, but amphibole inclusions in garnet are present in samples OSYB-14 and Ud79-27. According to the nomenclature (Leake et al., 1997), the amphibole is pargasite. The composition of amphibole varies in X_{Mg} from 0.52 to 0.57 (sample OSYB-9) up to 0.68–0.76 (OSYB-14 and Ud01-127), but remains rather close in TiO_2 content, 1.5 – 2.5 wt% (Supplementary Table 3). Amphibole inclusions in garnet from sample OSYB-14 contain up to 3.5 wt% TiO_2 content. Matrix amphiboles usually have higher $X_K = K/(K + Na)$ than do amphibole inclusions in garnet. The lowest X_K, 0.06 – 0.09, is recorded in a tiny amphibole inclusion in garnet intergrown with clinopyroxene in sample Ud01-127. Amphiboles contain detectable amounts of various volatiles. They are enriched in Cl (from 0.07 to 0.13 wt% in OSYB-14 up to 1.2 wt% in OSYB-9 and Ud01-127). Amphiboles from sample OSYB-14 show positive correlation between the Cl content and the K/(K + Na) ratio, which is typical for Cl-bearing amphiboles (Volfinger et al., 1985; Campanaro and Jenkins, 2017; Jenkins, 2019). Cl-bearing amphiboles from samples Ud01-127 and Ud79-27 contain up to 1.5 wt% F, which has negative correlation with chlorine. Amphiboles also contain SO_3 (up to 0.11 wt% in sample OSYB-9).

Scapolite is an accessory matrix mineral in sample OSYB-14 (Fig. 2c, g, and 3c). It has a Ca/(Ca + Na) ratio of 0.68 – 0.71, an SO_3 content of 2.3 – 4.6 wt%, and a Cl content of 0.07 – 0.3 wt% (Supplementary Table 3). According to the oxide totals, the CO_2 content in scapolite is 2.8 – 4.0 wt%.

Apatite in the studied samples occurs mainly as euhedral or subhedral inclusions in garnet, or rarely in other minerals (samples Ud01-127, Ud79-27, Ud79-24). Matrix apatites are found only in sample Ud01-300. The apatite is F-rich (2–4 wt%). The highest concentration of F was detected in apatite inclusions in garnet, in rim zones of matrix clinopyroxene, in plagioclase, and in F-Cl-bearing amphibole from sample Ud79-27. Chlorine content in apatite varies from 0.2 to 0.75 wt% (samples OSYB-14, Ud01-300, and Ud79-27) to about 2.5 wt% (Ud79-24 and Ud01-127). There is a rough negative correlation between F and Cl contents in apatites in each sample. Apatites also contain SO_3 varying from<0.1 wt% (Ud79-27) to 0.35–0.47 wt% (Ud01-127). The amount of SO_3 in apatites is positively correlated with Cl, which is known for magmatic apatites (e.g. Smith et al., 2012).

Accessory *ilmenite* with lamellae of *Ti-magnetite* of various thicknesses occurs both in the matrix and as inclusions in garnet. Ilmenite contains a hematite component in the range of 10–15 mol.%, whereas the ulvospinel content in Ti-magnetite varies between 12 and 50 mol.%. Composition of ilmenite is independent on its occurrence in the rock (matrix vs. inclusion). Compositional zoning of ilmenite in contact with the Ti-magnetite lamellae is commonly absent. However, tiny rims (up to 5 μm) of newly-formed Ti-magnetite were detected at the contact with kimberlite veinlets (e.g. Fig. 3e).

5. *P-T-f_{O2}* conditions of metamorphism

5.1. *Phase equilibria modeling*

The PERPLE_X software (version 6.8.3, updated on 18 Jun 2019), including database files 'hp62ver.dat' with a thermodynamic dataset and 'solution_model_686.dat' for solid-solution models, was used to construct phase diagrams for the samples of mafic granulite xenoliths from the Udachnaya kimberlite pipe. The modeling was carried out using the following solid solution models: Gt(HP) for garnet (Holland and Powell, 1998), Cpx(HP) and Opx(HP) for clinopyroxene and
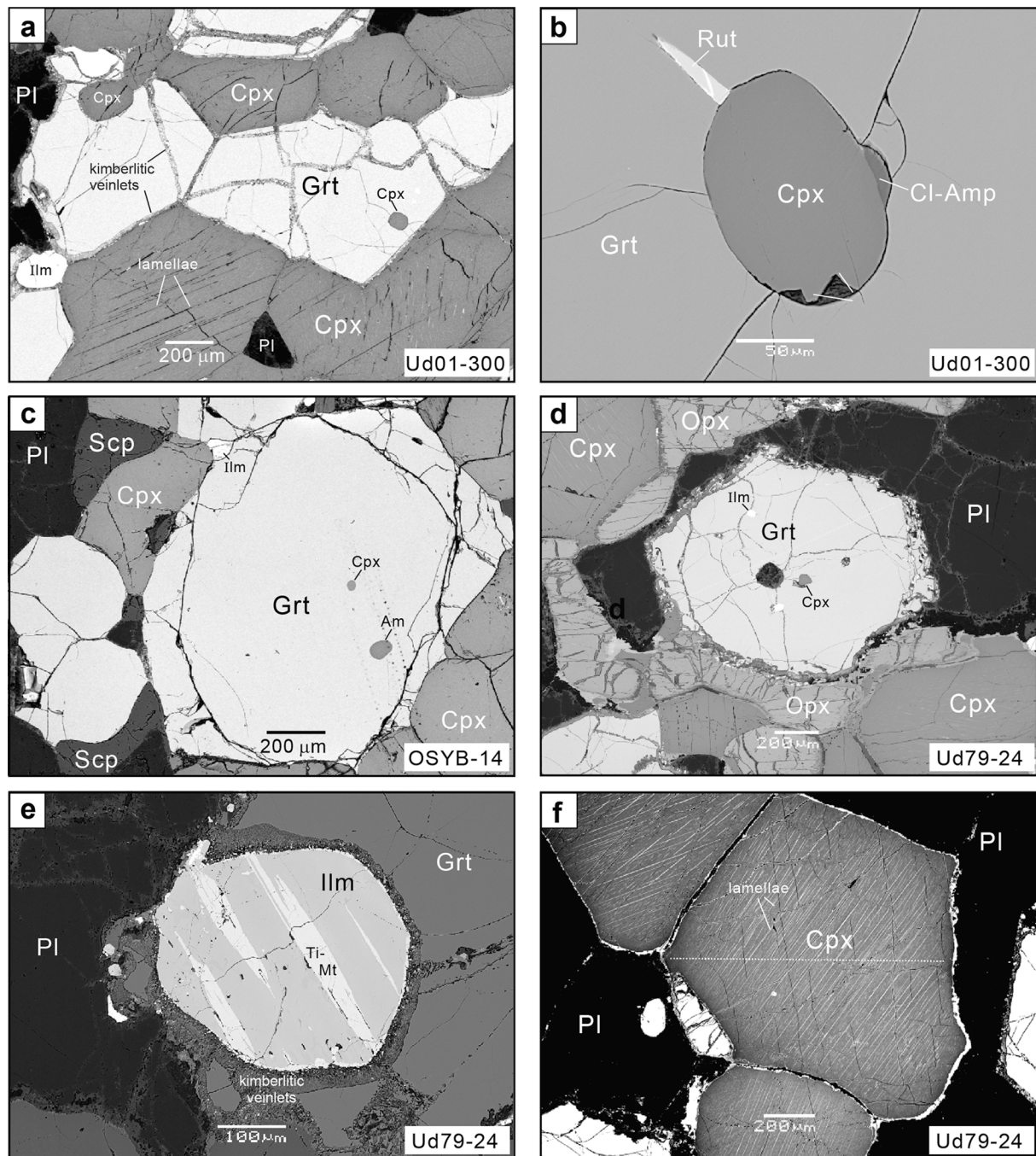
Fig. 3. Textural relations in the studied mafic granulite xenoliths. (a) Granoblastic texture and kimberlite-related veinlets crosscutting subhedral garnet grains. Note an incomplete trapping of clinopyroxene by garnet (at the left-hand side of the image). (b) A rounded clinopyroxene inclusion intergrown with minute amphibole and rutile in garnet. (c) Equilibrium relationships of scapolite with rock-forming minerals. (d) Chain of orthopyroxene grains between clinopyroxene, plagioclase, and garnet. (e) Inclusion of rounded ilmenite grain with Ti-magnetite lamellae in garnet. Note, newly-formed ilmenite in developed in the ilmenite rim at the contact with kimberlitic veinlet. (f) Lamellae-bearing clinopyroxene cores and lamellae-free rims of clinopyroxene grains. Yellow dotted lines mark positions of electron microprobe profiles. Sample numbers are shown in the BSE images.

orthopyroxene (Holland and Powell, 1996), feldspar for plagioclase (Fuhrman and Lindsley, 1988), cAmph(G) for amphibole (Green et al., 2016), and Melt(JH) for melt (Jennings and Holland, 2015).

We assumed that the effective composition of the studied mafic granulite xenoliths is more appropriate for the phase equilibrium modeling than the bulk composition obtained using XRF since the xenoliths were affected by the kimberlite-related alteration. The effective composition of each sample was quantified using modes of minerals (as number of pixels in a representative BSE image), and the density and composition of each mineral. Average compositions of zoned garnets and clinopyroxenes were calculated based on compositional profiles using the following equation

$$\overline{X} = \frac{\sum_{i=1}^{n} x_i * R_i^2 * \Delta x_i}{\sum_{i=1}^{n} R_i^2 * \Delta x_i}$$

where i = number of profile step, n = the amount of steps in the profile, x_i = composition of the mineral at step i, R_i = radial distance of step i, and Δx_i = size of the step i.

Calculated T-lgf_{O2} diagrams at different pressures revealed that the
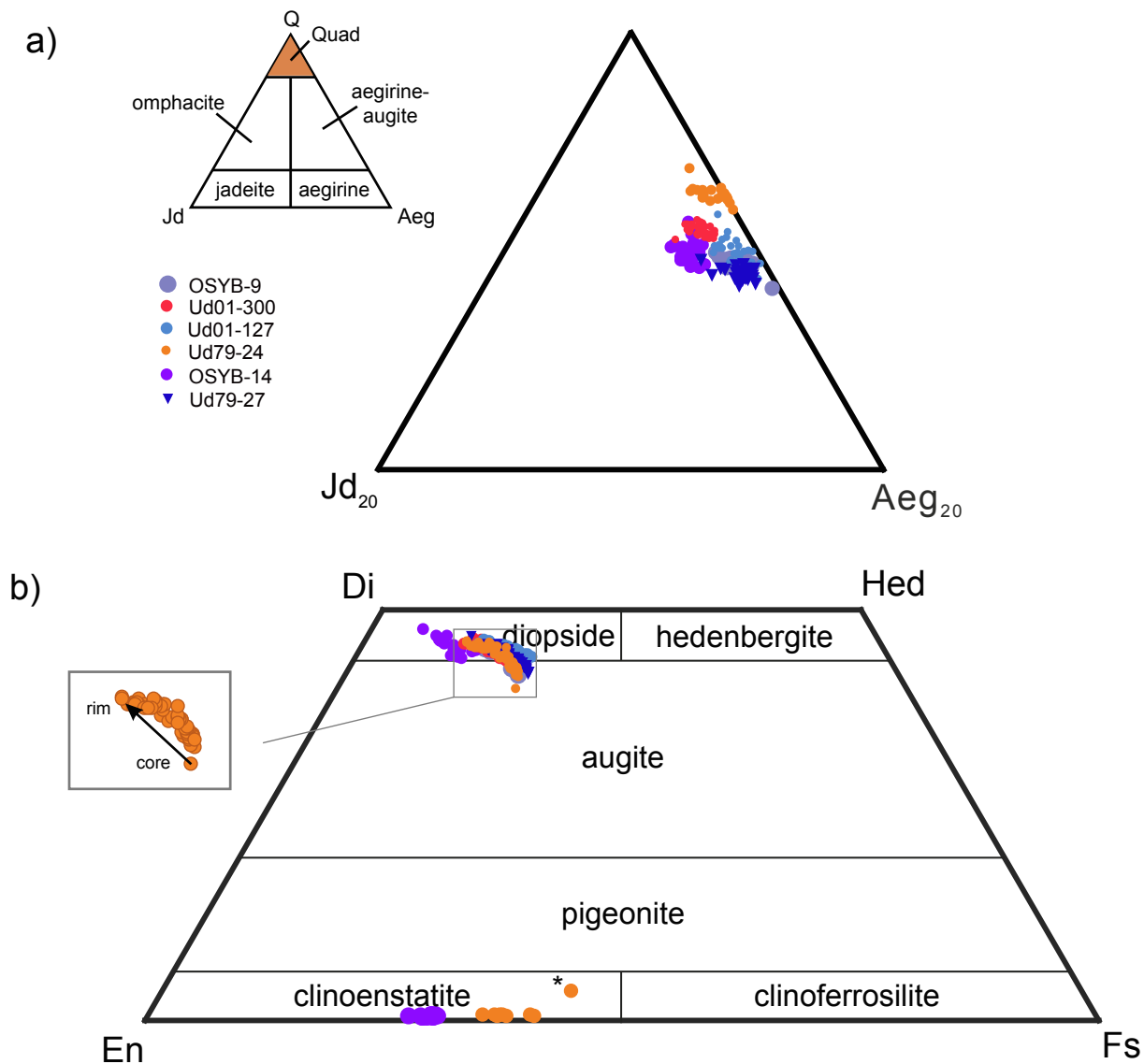
Fig. 4. Composition of clinopyroxene from the studied xenoliths plotted on the classification diagrams by Morimoto (1988). (a) Diagram for Ca-Mg-Fe and Na pyroxenes. Quad represents the Ca-Mg-Fe pyroxene area. (b) Diagram for Ca-Mg-Fe clinopyroxenes.

effective compositions of the samples with whole clinopyroxene grains were unable to reproduce the equilibrium compositions of coexisting clinopyroxene, plagioclase, and garnet (e.g. Supplementary Fig. 2, equilibrium analyses of the minerals are in Supplementary Tables 1–3). Therefore, we assumed that the problem arises from the effective compositions, which erroneously incorporate magmatic clinopyroxene cores (Shatsky et al., 2005) for modeling metamorphic equilibria in the rocks. Therefore, the lamellae-bearing cores of clinopyroxenes were excluded from the effective bulk compositions and only metamorphic lamellae-free rim zones of the clinopyroxenes were used (~10% of the radius, Table 2). H_2O and CO_2 were added only to the effective composition of sample OSYB-14, which contained rock-forming scapolite and amphibole. TiO_2 was used only for ilmenite and magnetite. Pyroxenes and garnets contain only a minor amount of TiO_2, which is not accounted for in the related solid solution models implemented in PERPLE_X. The effective bulk rock compositions of the studied samples utilized in the modeling are shown in Table 2.

Thermodynamic conditions of the rock's equilibration were reconstructed using calculations of T-f_{O2} (at constant pressure) and, subsequently, P-T phase diagrams. Each P-T diagram was quantified for a constant amount of oxygen unraveled from the appropriate value of f_{O2}

at the T-f_{O2} diagram via the *meemum* option of the PERPLE_X software. For each effective bulk composition, we searched for the appropriate mineral parageneses and compositional parameters of rock-forming minerals such as $X_{Mg} = Mg/(Mg + Fe)$, X_{Jd} (mole fraction of jadeite), and X_{Aeg} (mole fraction of aegirine) in clinopyroxene; $X_{Mg} = Mg/(Mg + Fe)$ and $X_{Ca} = Ca/(Ca + Mg + Fe)$ in garnet; $X_{Mg} = Mg/(Mg + Fe)$ in orthopyroxene; and $X_{An} = Ca/(Ca + Na + K)$ in plagioclase.

Phase equilibrium modeling was applied to all studied samples of granulite xenoliths. The reconstructed P-T-f_{O2} equilibrium parameters are presented in Table 2. Details of the reconstructions are presented in the T-lg(f_{O2}) and P-T diagrams for the samples with different mineral parageneses; Grt + Cpx + Pl + Ilm + Rt (Ud01-300), Opx + Grt + Cpx + Pl + Ilm (Ud79-24), and Grt + Cpx + Pl + Amp + Scp + Ilm (OSYB-14) (Fig. 9). Phase diagrams for the other samples are presented in Supplementary Fig. 3. Intersection of isopleths of mineral compositions in the P-T area with the appropriate mineral paragenesis was considered as equilibrium P-T-f_{O2} conditions for a rock. Compositions of the minerals from all samples (Tables 2 and 3) match the model compositions at temperatures 620–660 °C, pressures 0.9–1.0 GPa and lgf_{O2} = −21.4 to −19.5 (Table 2, Fig. 9, Suppl. Fig. 2), i.e. 2.0–2.5 log units below the FMQ buffer. These P-T estimates are localized at the low-temperature
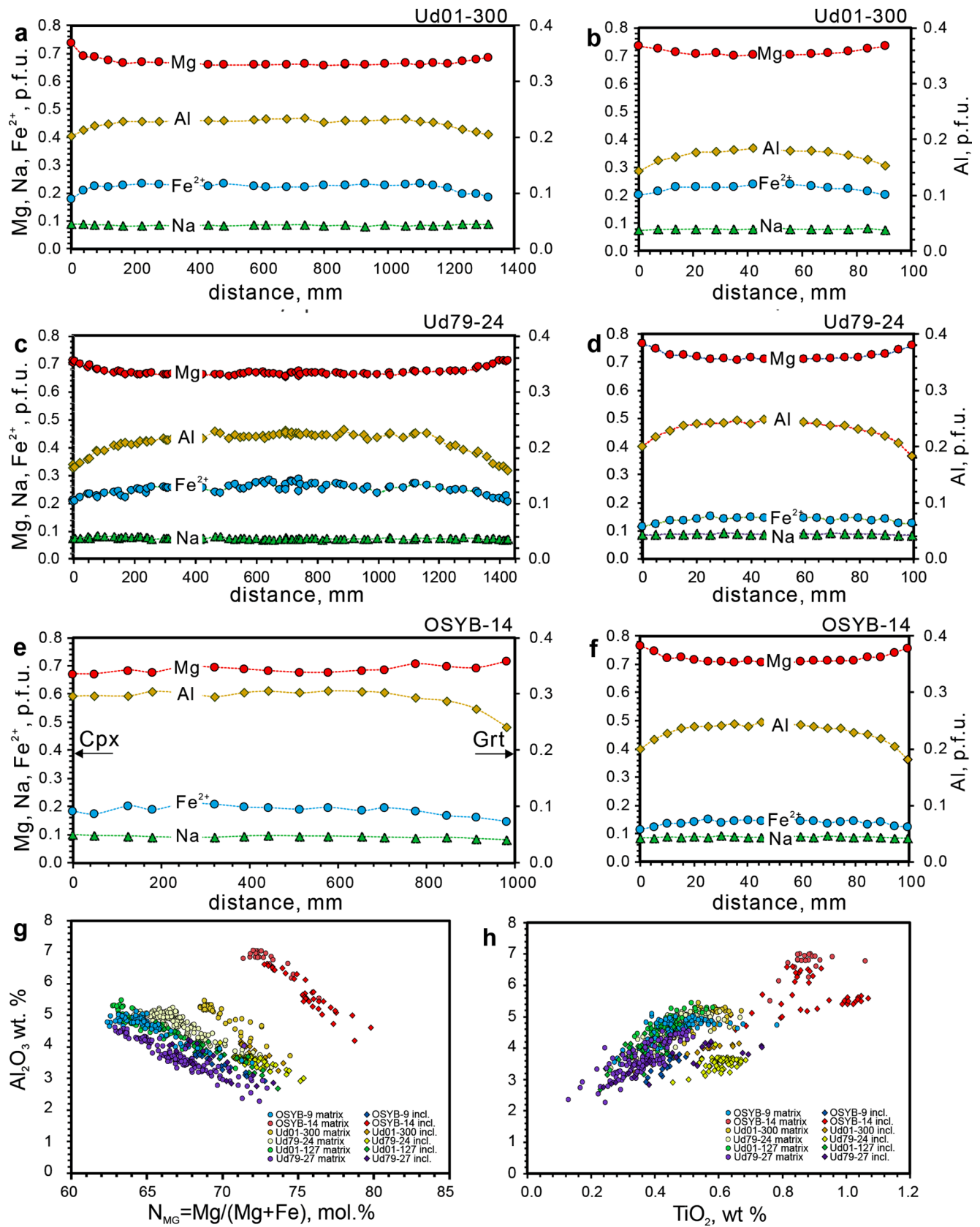
Fig. 5. Composition of clinopyroxene in the matrix grains and in the inclusions in garnet from the studied granulite xenoliths. Compositional profiles in sample Ud01-300 (a-b), Ud79-24 (c-d), and OSYB-14 (e-f). Plots of Al_2O_3 (wt%) against N_{Mg} (g) and TiO_2 (wt%) (h). Note, Al content in the (a-f) profiles is shown on the secondary axis.
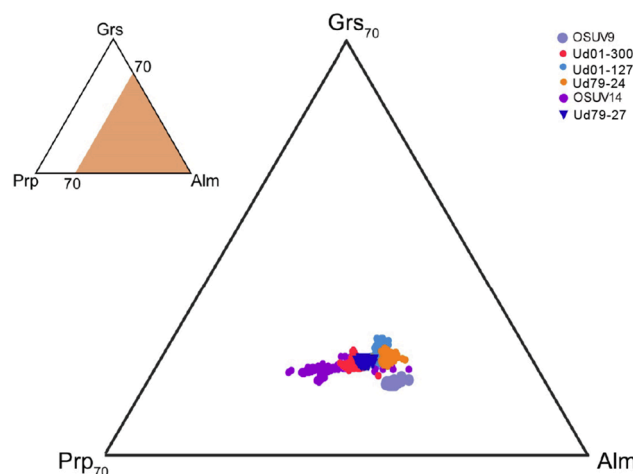
Fig. 6. The Prp-Grs-Alm diagram for garnets from the studied mafic granulite xenoliths.

and high-pressure boundary of the large P-T array, which was framed by previous geobarometric estimates for the xenoliths of the Udachnaya kimberlite pipe (Fig. 10a).

5.2. Conventional geothermobarometry

Temperatures of the mafic xenoliths equilibration were reconstructed using garnet-clinopyroxene (Ellis and Green, 1979; Ai, 1994; Ravna, 2000) and garnet-orthopyroxene (Harley, 1984) geothermometers for the rim compositions of contacting minerals (located away from kimberlite veinlets) at the pressure obtained from the phase equilibrium modeling. All the Fe-Mg minerals were treated as Fe^{3+}-free phases following the requirements of corresponding versions of the geothermometers. The obtained temperatures fall in the range of 540–700 °C (Fig. 10a, Table 3), which agrees with the results of the phase equilibrium modeling (620–660 °C, Table 2, Fig. 9 b, c, d).

The garnet-plagioclase-clinopyroxene-quartz geobarometer (Newton and Perkins, 1982) as a key sensor of pressure for the mafic granulites from the Udachnaya kimberlite pipe was applied to the sample (Ud01-127) in which quartz was detected as a minute phase. The obtained pressure of ~0.6 GPa is lower than that obtained using phase equilibrium modeling and previous pressure estimates on mafic granulites from the Udachanya kimberlite pipe (Fig. 10a). A problem of applying the garnet-plagioclase-clinopyroxene-quartz geobarometer to the mafic granulite xenoliths is discussed in section 6.2.

5.3. Ti-oxide oxythermometry

Application of the magnetite-ilmenite oxythermometer by Anderson and Lindsley (1985) implemented into the ILMAT Excel spreadsheet (Lepage, 2003) to the compositions of Ti-bearing magnetite-ilmenite intergrowth provides temperature in the range of 850–990 °C and lgf_{O2} between −10 and −12, i.e. at the level FMQ ± 0.5 (Fig. 10b). These values differ from those inferred from silicate rock-forming minerals and are likely related to an earlier stage of rock evolution (see below).

6. Discussion

6.1. Mineral reactions and equilibria

Initial stages of garnet growth in high-grade metaigneous basic rocks are well documented as corona structures (Griffin and Heier, 1973; McLelland and Whitney, 1980; Keller et al., 2008; Ashworth et al., 1998; Perchuk and Morgunova, 2014). These structures are composed of single or multiple shells of mineral(s) between felsic and Fe-Mg domains of the

rocks due to the opposite diffusion fluxes of Ca and Al vs Fe and Mg caused by gradients of chemical potentials (Keller et al., 2008; Ashworth et al., 1998). Usually, only rim zones of Fe-Mg minerals (pyroxenes, olivine) participate in the corona formation, whereas their magmatic cores remain unreacted and isolated from the other metamorphic minerals (Griffin and Heier, 1973). In contrast, plagioclase is often extensively or totally recrystallized and replaced by a new metamorphic assemblage (e.g. McLelland and Whitney, 1980; Perchuk and Morgunova, 2014).

Corona structures are rare in mafic crustal xenoliths (Rudnick, 1992; Pearson et al., 1995). They are absent in the granulite xenoliths of the Udachnaya pipe (Shatsky et al., 2019 and references therein; Koreshkova et al., 2009; Moyen et al., 2017). Although our samples are corona-free, this stage cannot be excluded from their early evolution, when isolation of magmatic cores of clinopyroxene and recrystallization of plagioclase occured.

Mineral reactions in the mafic xenoliths are predominantly recorded in zoning of rock-forming minerals, as well as by inclusions in garnet and the composition of those inclusions. In all studied samples, compositions of clinopyroxene inclusions in garnet correspond only to the compositions of the rim zones of matrix grains with respect to Mg-number and CaO and Al_2O_3 contents (Fig. 5). Thus, only rim zones of matrix clinopyroxene grains (Cpx$_2$) were equilibrated with the growing garnet according the generalized scheme

$$Pl_1 + Cpx_1 \rightarrow Grt + Cpx_2 + Pl_2, \tag{1}$$

where Cpx_1 is a remnant of the initial igneous clinopyroxene that comprises the cores of the matrix grains, Cpx_2 is a newly formed metamorphic clinopyroxene in the rim zones of matrix grains and clinopyroxene inclusions in garnet, Pl_1 is initial igneous plagioclase, which was likely recrystallized and partially reacted-out, and Pl_2 is newly formed metamorphic plagioclase. New generations of clinopyroxene and plagioclase are enriched in diopside and albite, respectively.

Formation of garnet after clinopyroxene and plagioclase is commonly ascribed to the end-member reactions

$$An + Di = 2/3Grs + 1/3Prp + Qz, \tag{2}$$

$$An + Hd = 2/3Grs + 1/3Alm + Qz. \tag{3}$$
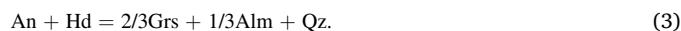
The positive Clapeyron slope of these reactions (Newton and Perkins, 1982; Moecher et al., 1988) implies garnet growth due to the increase of pressure and/or decrease of temperature. These reactions were used to estimate pressure for the mafic granulites using a garnet-plagioclase-clinopyroxene-quartz geobarometer (Shatsky et al., 2005, 2016, 2019; Koreshkova et al., 2011). Since quartz is absent in most of our studied samples or its amount is negligible, the garnet growth is supposed to be controlled by quartz-free reactions. Widespread ilmenite-Ti-magnetite inclusions in garnet suggests the following garnet-forming reactions

$$2An + Hd + 2Usp = Grs + Alm + 2Ilm, \tag{4}$$

$$2An + Di + 2Usp = Grs + 2/3Alm + 1/3Prp + 2Ilm. \tag{5}$$
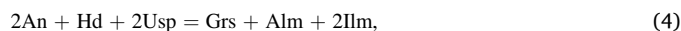
Reactions (4) and (5) also have a positive Clapeyron slope (similar to reactions (2) and (3)), and, thus, produce garnet via an increase of pressure and/or cooling. Consumption of ulvospinel from the magnetite-ulvospinel solid solution is interpreted as indicating that the mineral equilibrium

$$3Usp + 1/2O_2 = Mag + 3Ilm \tag{6}$$

is shifted to the right during cooling (e.g. Anderson and Lindsley, 1985). Simultaneously operating reactions (4) - (6) explain formation of garnet without quartz as well as consumption of oxygen from the fluid phase, thus creating reduced conditions in a fluid-deficient environment.

Elevated TiO_2 content in garnet (0.09–0.16 wt%) indicates that Ti-bearing oxides also participated in the garnet-forming end-member
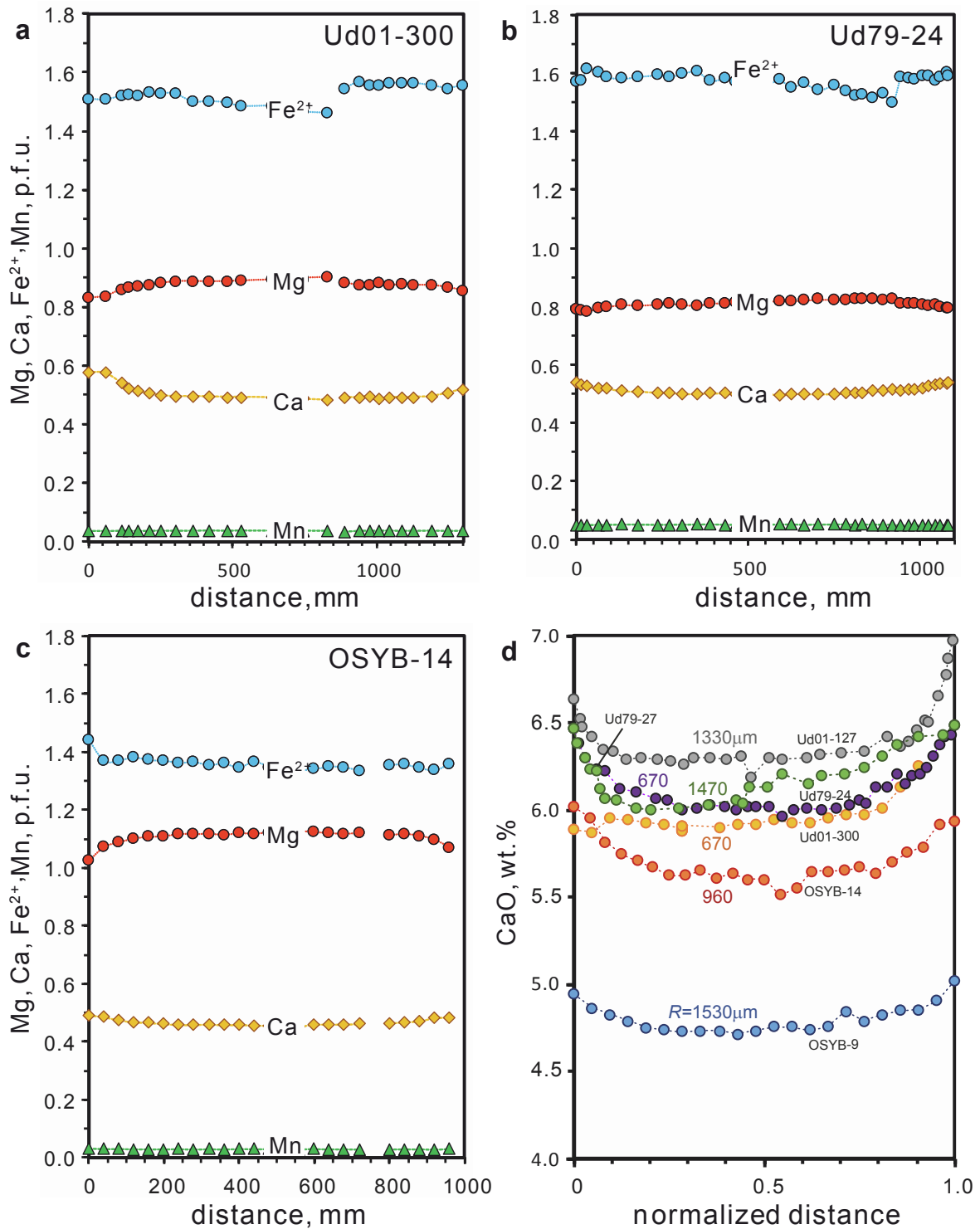
Fig. 7. Compositional profiles across garnets from the studied granulite xenoliths. Profiles are shown for divalent cations in sample Ud01-300 (a), Ud79-24 (b), and OSYB-14 (c). CaO (wt%) zoning profiles normalized to the size of the garnet grains from different samples (d).
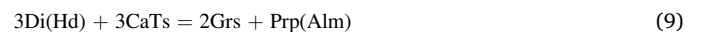
reactions, e.g.

$$An + 2Di + Usp = Ti\text{-}Mg\text{-}Grt + 2/3Alm + 1/3Prp, \qquad (7)$$

$$An + 2Hd + Usp = Ti\text{-}Fe\text{-}Grt + 2/3Alm, \qquad (8)$$

where Ti-Mg-Grt is a model Mg-morimotoite end-member, $Ca_3Ti\text{-}MgSi_3O_{12}$, and Ti-Fe-Grt is an Fe-morimotoite end-member, $Ca_3TiFe^{2+}Si_3O_{12}$.

Minor end-members of the clinopyroxene solid solution might also

contribute to garnet growth owing to various reactions. For example, reaction

$$3Di(Hd) + 3CaTs = 2Grs + Prp(Alm) \qquad (9)$$

explains the regular decrease of Al_2O_3 in clinopyroxene (Ca-Tschermak molecule) toward the rims (Fig. 5a, c), whereas reaction

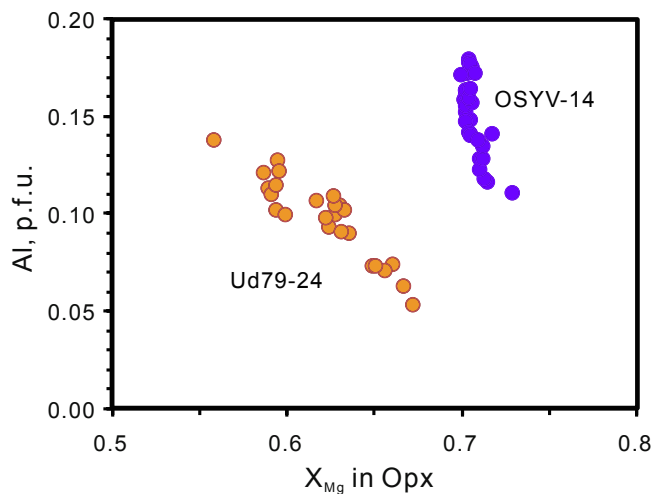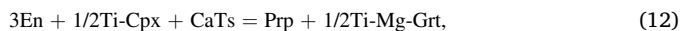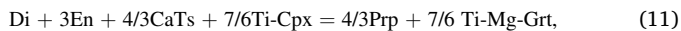$$3En(Fs) + 3CaTs = Grs + 2Prp(Alm) \qquad (10)$$
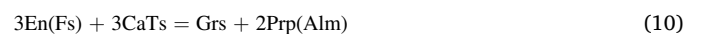
Fig. 8. Composition of orthopyroxene of the studied granulite xenoliths on the X_{Mg}-Al plot.

shows a consumption of the enstatite end-member, which agrees well with the disappearance of low-Ca pyroxene lamellae in rim zones of clinopyroxene grains (Fig. 3f). Formation of the Ti-bearing garnet end-member could also proceed (as an addition to reactions 7 and 8) at the expense of minor components in the igneous clinopyroxene according to the reactions:

$$Di + 3En + 4/3CaTs + 7/6Ti\text{-}Cpx = 4/3Prp + 7/6 \text{ Ti-Mg-Grt}, \quad (11)$$

$$3En + 1/2Ti\text{-}Cpx + CaTs = Prp + 1/2Ti\text{-Mg-Grt}, \quad (12)$$

where Ti-Cpx is the model Ti-bearing clinopyroxene end-member $CaMgTiSiO_6$ (Ca-Ti-Tschermack molecule). Clinopyroxene grains indeed show a decrease of the TiO_2 content toward the rims (Supplementary Table 1). Although the standard thermodynamic properties of the Ti-bearing garnet and clinopyroxene end-members are unknown, rough thermodynamic analysis shows that reactions (9–12) could also displace to the right upon cooling, similar to all the above reactions.

Reactions with participation of ore minerals can explain the coexistence of garnet with SO_4-scapolite in sample OSYB-14, e.g.

$$15An + Po + 6Hd + 4Mt = 19/3Alm + 17/3Grs + SO_4\text{-Scp}. \quad (13)$$
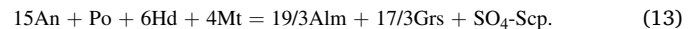
This reaction generally illustrates a mechanism of sulfate-scapolite formation during metamorphism of igneous cumulates with sulfur sourced from precursor igneous sulfides, which was suggested on the basis of S-isotopic analyses of scapolites from mafic crustal xenoliths (Hammerli et al., 2017). Note that reaction (13) does not require participation of a fluid to stabilize the sulfate component in scapolite.

Garnets in the studied xenoliths show slight concentric zoning in terms of both high-diffusivity Fe and Mg and low-diffusivity Ca (Fig. 7, Perchuk et al., 2009). Such a zoning pattern is likely attributed to the garnet growth rather than to the diffusion exchange with co-existing minerals for the following reasons. (1) The Fe-Mg exchange between garnet and pyroxenes should produce Fe-Mg zoning in the garnet rims rather than the Mg-Ca zoning observed in the studied grains (Fig. 7). (2) Mg-Ca zoning in garnet at the contact with plagioclase cannot be related to the cation exchange between these minerals, because plagioclase is an Mg-free mineral. (3) As emphasized by Koreshkova et al. (2011), compositional zoning in clinopyroxene rims is much wider than zoning in garnet rims (cf. Figs. 5 and 7), which is opposite to the Fe-Mg self-diffusion coefficients in the minerals (Perchuk et al., 2009; Müller et al., 2013). (4) Zoning of clinopyroxene is expressed not only in Fe and Mg, but also in Al, which also cannot participate in the exchange reaction.

Nevertheless, the temperature sensitive Fe-Mg exchange reaction

$$Prp + 3Hd = Alm + 3Di \quad (14)$$

most likely controlled compositions of the coexisting garnet and clinopyroxene during cooling of the mafic granulites.

6.2. Oxygen fugacity in the crustal granulites

Data on the redox conditions in lower-middle crustal xenoliths are extremely scarce. To our knowledge, the redox conditions were discussed only for sapphirine-bearing metapelite xenoliths from the Lace Kimberlite, Kaapvaal Craton (Dawson and Smith, 1987) and for mafic granulite xenoliths from the Bakony–Balaton highland volcanic field, Hungary (Török et al., 2005). Dawson and Smith (1987) suggested

Table 2
Effective bulk compositions (without and with cpx cores) and reconstructed P-T-f_{O2} conditions of the samples of granulite xenoliths from Udachnaya kimberlite pipe.

| Sample	SiO$_2$	TiO$_2$	Al$_2$O$_3$	FeO	MnO	MgO	CaO	Na$_2$O	H$_2$O[**]	CO$_2$[**]	#Mg	Cpx, %R[*]	P, GPa	T, °C	lg (fO$_2$)	lg (QFM)	log (fO$_2$-QFM)	O$_2$, wt%
cpx cores excluded																		
OSYB9	45.08	2.78	20.28	17.81	0.37	3.75	6.70	2.96	–	–	0.27	15	0.9	650	−20.5	−18.0	−2.5	0.03
OSYB14	44.52	1.84	21.21	13.16	0.22	6.92	8.41	2.43	0.27	0.15	0.48	10	0.8	600	−20.5	−19.6	−0.9	0.03
Ud01-127	46.12	3.13	20.91	14.93	0.30	3.10	7.05	3.60	–	–	0.27	10	0.9	640	−21.4	−18.3	−3.1	0.02
Ud01-300	44.26	2.34	21.23	17.92	0.34	4.59	6.53	2.55	–	–	0.31	5	0.9	650	−20.8	−18.0	−2.8	0.01
Ud79-24	46.50	1.49	19.84	15.90	0.37	5.84	6.87	2.59	–	–	0.40	10	0.9	660	−21.0	−17.7	−3.3	0.01
Ud79-27	48.06	2.40	20.74	13.70	0.31	3.61	6.97	3.89	–	–	0.32	10	1.0	650	−19.5	−17.9	−1.6	0.03
cpx cores is included																		
OSYB9	46.88	2.05	15.36	15.60	0.29	6.18	10.97	2.47	–	–	'							
OSYB14	45.99	1.57	17.20	11.77	0.17	8.45	11.77	2.12	0.19	0.11	0.56							
Ud01-127	47.45	2.33	16.12	13.82	0.21	5.50	10.94	2.98	–	–	0.41							
Ud01-300	46.55	1.70	15.39	14.85	0.25	7.30	11.74	2.05	–	–	0.47							
Ud79-24	46.48	1.49	19.86	15.93	0.37	5.83	6.85	2.59	–	–	0.39							
Ud79-27	49.26	1.63	14.31	12.63	0.23	6.65	12.12	2.96	–	–	0.48							

* size of the Cpx rim zone in the effective composition, % of the radius.
** quantified on the basis of amphibole (H2O) and scapolite (CO2) modes.
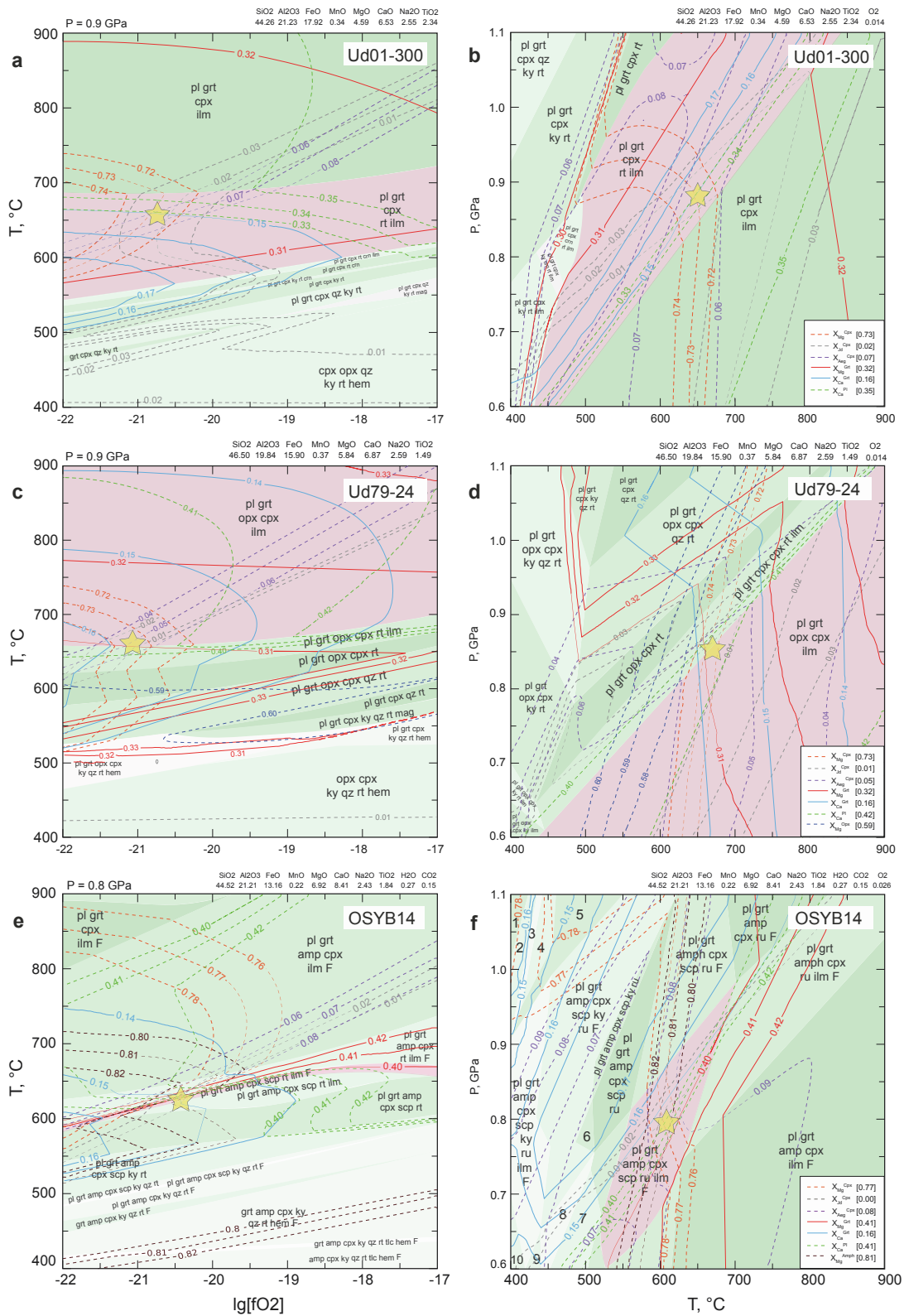
Fig. 9. Results of phase equilibria modeling for the effective compositions of the studied samples. (a) T-lg(f_{O2}) diagram at P = 0.9 GPa for the mafic granulite Ud01-300; (b) P-T diagram for the mafic granulite Ud01-300 with O$_2$ = 0.014 wt%; (c) T-lg(f_{O2}) diagram at P = 0.9 GPa for the mafic granulite Ud79-24; (d) P-T diagram for the mafic granulite Ud74-24 with O$_2$ = 0.014 wt%; (e) T-lg(f_{O2}) diagram at P = 1.0 GPa for the mafic granulite OSYB-14; (f) P-T diagram for the mafic granulite OSYB-14 with O$_2$ = 0.025 wt%. Phase diagrams show mineral assemblages calculated for the effective rock compositions shown above the plots. Color code for the isopleths of the minerals and related equilibrium compositions is shown in the inset of the P-T diagrams (b, d, f). Stars show equilibrium T-fO_2 and P-T conditions in the fields of appropriate mineral parageneses. See text for details.
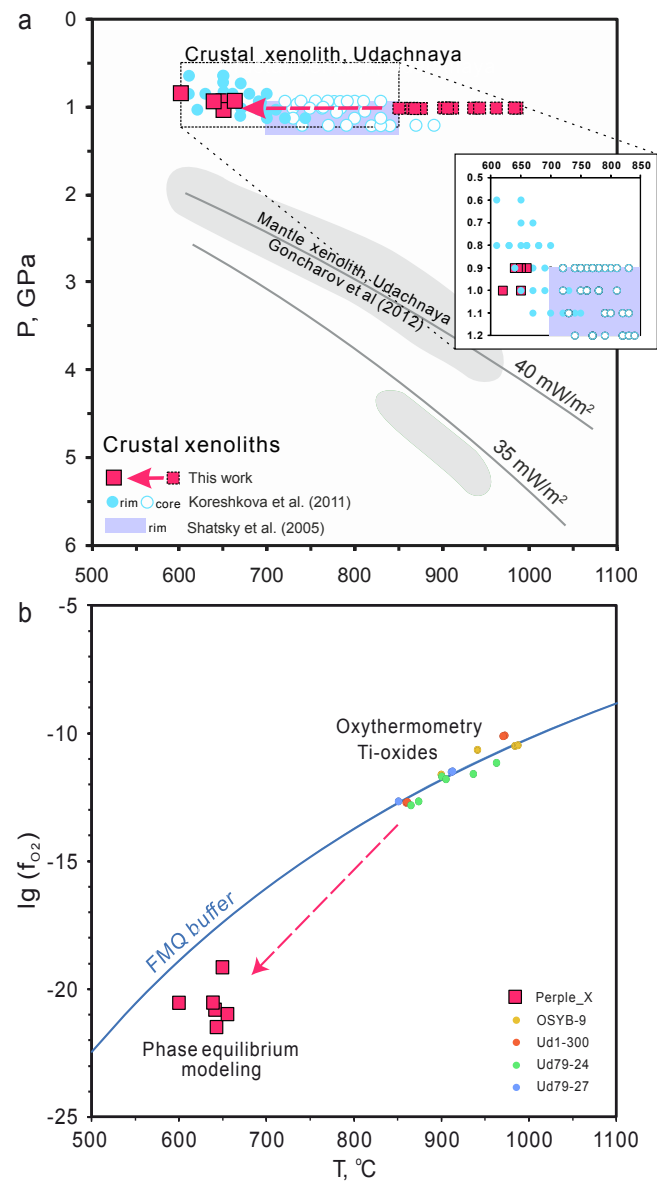
Fig. 10. Thermodynamic conditions of the tectono-thermal events recorded by the granulite xenoliths from the Udachnaya kimberlite pipe. (a) P-T conditions and possible P-T path for the studied samples obtained using the phase equilibrium modeling and Ti-oxide oxythermometry (red squares) in comparison to the previous P-T estimates for mafic granulite xenoliths (Shatsky et al. 2005; 2016, Shatsky et al., 2019; Koreshkova et al., 2011) and mantle xenolith (Goncharov et al., 2012) from the Udachnaya kimberlite pipe (Fig. 9, Tables 2 and 3). (b) Evolution of T-lg(fO_2) conditions of the studied samples obtained using the phase equilibrium modeling and the Ti-oxide oxythermometry.

(without quantitative evaluation) reduced conditions based on the coexistence of graphite and sulfides as well as an absence of Fe^{3+} in silicate minerals and concluded that such conditions were imposed by the chemical composition of the metapelite protolith. Török et al. (2005) inferred fO_2 2.5–2 log units below FMQ based on the CO_2-CO-graphite inclusions in plagioclase and pyroxene in the mafic granulite xenoliths. Redox conditions have never been reported for crustal xenoliths from the Yakutian kimberlites.

Our study revealed relatively high aegirine content in clinopyroxenes from representative samples of the mafic granulites (Supplementary Table 1). Since the aegirine content is dependent on fO_2 (e.g. Redhummer et al., 2000), one can consider the aegirine-bearing clinopyroxenes as evidence for oxidized conditions. However, the phase

Table 3
Results of conventional thermobarometry of the samples of granulite xenoliths from the Udachnaya kimberlite pipe.

Sample	Cpx X_Mg	Cpx X_Jd	Cpx X_Aeg	Grt X_Mg	Grt X_Ca	Opx X_Mg	Opx Al$_2$O$_3$	Geothermometry*, °C Cpx-Grt (Ai, 1994)	Cpx-Grt (Ravna, 2000)	Cpx-Grt (Ellis& Green, 1979)	Opx-Grt (Harley, 1984)	Geobarometry, GPa Grt-Pl-Cpx-Qz (Newton & Perkins, 1982)	Modeling Perple_X P, GPa	T, °C
OSYB9	0.68	0.02	0.08	0.27	0.14	–	–	593	605	702	–	–	0.9	650
OSYB14	0.77	0.00	0.08	0.41	0.16	0.72	3.24	633	649	767	641	–	0.8	600
UD-79-24	0.73	0.01	0.05	0.32	0.16	0.59	2.27	604	617	719	724	–	0.9	660
UD-79-27	0.67	0.02	0.09	0.27	0.17	–	–	648	653	744	–	–	1.0	650
UD-01-127	0.70	0.01	0.09	0.28	0.19	–	–	632	638	733	–	0.6	0.9	640
UD-01-300	0.73	0.02	0.06	0.32	0.16	–	–	604	617	719	–	–	0.9	650

* at pressure from the modeling results.

equilibrium modeling for all samples demonstrated that such clinopyroxene compositions were formed under reduced conditions (1.6–3.3 log units below FMQ buffer) at 600–650 °C and 0.8–1.0 GPa at the final stage of granulite equilibration (Supplementary Table 3).

Ti-oxides in the studied rocks indicate relatively high temperatures, 850–990 °C, and f_{O2} close to the FMQ buffer (Fig. 10b), conditions which likely correspond to an earlier episode of rock formation. High-grade rocks from regional metamorphic complexes typically show f_{O2} close to or above the FMQ buffer (Bohlen and Essene, 1977; Lamb and Valley, 1984; Skippen and Marshall, 1991; Harlov, 1992, 2000). However, reduced f_{O2} (down to 3 log units below the FMQ buffer) were established for some large igneous complexes (e.g. Nain, Adirondacks, Quebec, and Scouri) which experienced high-grade metamorphism (Berg, 1977; Lamb and Valley, 1984; Skippen and Marshall, 1991; Valley et al., 1990). Lamb and Valley (1984) and Valley et al. (1990) highlighted several specific petrological and mineralogical features of the rocks from such metaigneous complexes. In addition to the reduced f_{O2}, they show simultaneously low H_2O and CO_2 activities, strong oxygen isotope gradients, and high Cl and F contents in hydrous minerals. All these features are assumed to be inherited from the magmatic precursors, which underwent devolatilization before or during the onset of the fluid-deficient metamorphism (Berg, 1977; Valley et al., 1990; Skippen and Marshall, 1991). The arguments in the next section show that reduced conditions in the studied granulite xenoliths were also, probably, a result of the fluid-deficient metamorphism.

Although re-equilibration of Ti-oxides is relatively quick (Hammond and Taylor, 1982) at temperatures of kimberlite melts (970–1100 °C at pressures ~1 GPa, e.g. Fedortchouk et al., 2005), oxythermometry of Ti-oxides in the studied samples shows much more oxidized conditions (at the level of the FMQ buffer at ~1000 °C) than those of a kimberlite melt (3 log units below FMQ buffer at 1000 °C and ~1 GPa, Fedortchouk et al., 2005). Accordingly, we assume that thermal effect of the kimberlite magma on the compositions of ilmenite and magnetite in the xenoliths was insignificant.

6.3. Fluid: small amount but complex composition

According to the phase equilibria modeling (not included in the paper), the modal amount of amphibole positively correlates with the amount of a hydrous fluid in the effective composition. Accordingly, the very limited mode (or even the lack) of amphibole in the studied rocks under the amphibolite facies conditions is considered as definitive evidence for a deficit of hydrous fluid during the rock equilibration. We suggest that this feature could be a consequence of an initial deficit of H_2O in the mafic magmas extracted from the relatively dry subcontinental mantle and subsequent evolution of the rocks without voluminous influx of external fluids. In contrast, if metabasic rocks evolved during sagduction of greenstone material they might bring to the depths a relatively high amount of H_2O stored in hydrous minerals (e.g. amphibole, epidote).

Fluid species during equilibration of the studied granulites were calculated using the *fluid.exe* module of the PERPLE_X software for the C-O-H system at the most common (0.9 GPa/650 °C) and the lowest (0.8 GPa/600 °C) P-T conditions reconstructed from the studied samples for a wide range of f_{O2} (Fig. 11). The MRK EoS equation for fluid species from Connolly and Cesare (1993) was applied. Following Valley et al. (1990), activity of graphite in graphite-free rock was set to 0.1. Calculations for the C-O-H fluid demonstrate that H_2O is a strongly predominant fluid species for samples Ud79-27 and OSYB-14 (Fig. 11), which agrees with the petrographic observations. For example, amphibole inclusions in garnet were found only in these rocks suggesting the presence of a hydrous fluid during garnet growth. In addition, the amphibole mode in sample OSYB-14 is the highest among the studied granulites. Lower f_{O2} in other samples (Table 2) corresponds to the higher amounts of CH_4 in the fluid. Amphibole is a minor phase (<1 vol%) in these samples, while amphibole inclusions in garnet are absent. This implies
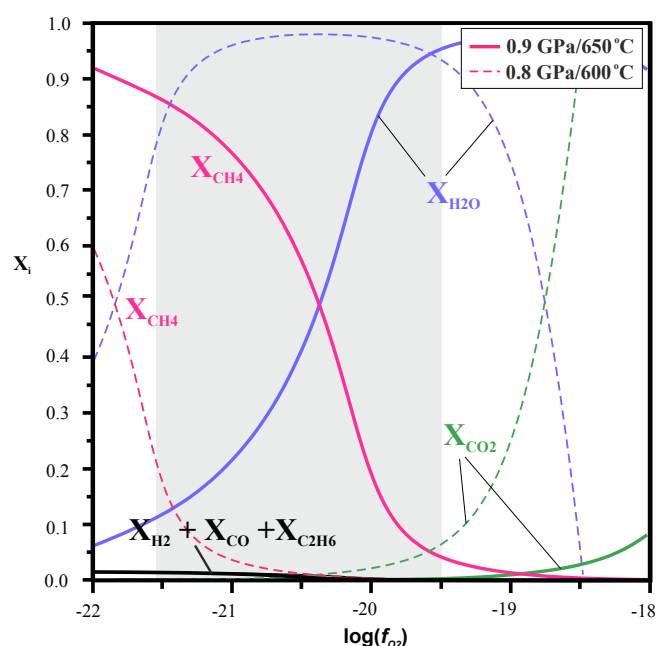

Fig. 11. Mole fractions of species (X_i) at most common (0.9 GPa/650 °C) and lowest (0.8 GPa/600 °C) P-T conditions in the studied samples at different f_{O2} in the C-O–H fluids. Shaded area: range of f_{O2} inferred from the phase equilibria modeling of the studied mafic granulites (Fig. 9, Table 2).

that hydrous fluid was deficient in these rocks. Additional textural evidence for that is the absence or extreme rarity of detectable fluid inclusions in minerals of the mafic xenoliths (V.S. Shatsky, unpublished data).

Electron microprobe analyses of amphiboles and accessory minerals provide a record of the rather complex composition of a possible metamorphic fluid. For example, amphiboles from the matrix and inclusions in garnets are enriched in Cl (up to 0.5 wt%) implying their growth in equilibrium with brines (Volfinger et al., 1985; Campanaro and Jenkins, 2017; Jenkins, 2019). Apatite inclusions in both garnet and metamorphic rims of clinopyroxene are Cl- and F-rich (samples UD01-127, UD79-27, UD79-24), further confirming halogen-rich environments.

Ti-oxides revealed crystallization temperatures of 850–990 °C, suggesting either a magmatic or a near-solidus origin. Sulfides (pyrrhotite, pyrite, chalcopyrite) might also be relics of this high temperature stage (e.g. Carmichael, 1991). During subsequent metamorphism sulfur was stored in amphibole (up to 0.11 wt% SO_3), apatite (0.1–0.47 wt% SO_3), and SO_4-bearing scapolite (2.3 – 4.6 wt% SO_3). Scapolite in the studied samples is sulfate-carbonate bearing, which is common for the mafic xenoliths from the Udachnaya pipe (Shatsky et al., 2005, 2016, 2019; Koreshkova et al., 2011), as well as for crustal xenoliths worldwide (e.g. Rudnick, 1992). The textural and compositional equilibrium of scapolite with garnet, clinopyroxene, plagioclase, and amphibole was reproduced as mineral paragenesis in the modeled phase diagram for sample OSYB-14 (Fig. 9e-f). The presence of SO_4^{2-} and CO_3^{2-} – bearing scapolite in the granulites implies the presence of both SO_2 and CO_2 in the metamorphic fluid. Further evidence for the elevated SO_2 content in the fluid during equilibration of the mafic granulites could be the sulfate component in apatite. Nevertheless, the presence of sulfate in minerals can result from a metamorphic reaction, such as (13), which does not involve fluid.

Thus, mineralogical data indicate that if a fluid phase existed during metamorphic reactions in the mafic granulites, it was represented by a small amount of a polyionic brine, which was able to impose low water activity, especially at pressures of the middle-lower crust (e.g. Aranovich and Newton, 1997; Manning and Aranovich, 2014). The brines could be exsolved from crystallizing basic melts (cf. Webster et al., 2018

and references therein). In a similar way, the SO_2 (and CO_2) degassing during crystallization is often taken to explain reduced conditions in (meta)magmatic rocks of basaltic composition (Anderson and Wright, 1972; Carmichael and Ghiorso, 1986; Carmichael, 1991; Kelley and Cottrell, 2012; Smith et al., 2012). Small portions of brines and reduced conditions could be further retained during subsequent crystallization and modification of minerals in the course of sub-isobaric cooling down to the temperature of final equilibrium at 600–650 °C. Such a feature seems to be typical for the fluid-deficient metamorphism in metaigneous complexes (e.g. Valley et al., 1990).

6.4. Granulites at nongranulitic P-T conditions

It is widely accepted that mafic granulites constitute a voluminous portion of the lower continental crust of the cratons (Bohlen and Mezger, 1989; Rudnick and Fountain, 1995). Previous thermobarometric studies of mafic granulite xenoliths from the Udachnaya kimberlite pipe revealed a broad range of metamorphic P-T conditions (Fig. 10a) corresponding mainly to granulite facies, and rarely to amphibolite facies metamorphic conditions in the lower and middle crust. Note, these data were obtained by using only conventional thermobarometric tools such as garnet-clinopyroxene (Ellis and Green, 1979; Powell, 1985; Ai, 1994; Ravna, 2000) and garnet-orthopyroxene (Wood and Banno, 1973) geothermometers, and garnet-plagioclase-clinopyroxene-quartz (Newton and Perkins, 1982) and clinopyroxene-plagioclase-quartz (Holland, 1983) geobarometers. These estimates agree with the P-T conditions obtained for crustal xenoliths from other Yakutian pipes (Shatsky et al., 2005; Koreshkova et al., 2009).

Phase equilibrium modeling of the mafic granulites from two different collections provide a record of a relatively narrow range of metamorphic temperatures and pressures (Fig. 9, 10a) that correspond to amphibolite facies metamorphic conditions. Although our data agree with some previous P-T estimates on the Udachnaya crustal xenoliths, they differ from most of the data (Fig. 10a). The differences may arise due to (1) differences in P-T equilibration of each xenolith, or (2) the use of mineral compositions associated with different growth stages. For example, we excluded data from the magmatic cores of the clinopyroxenes when deciphering metamorphic P-T conditions; data from such cores provide the highest temperatures and pressures reported in previous studies (Fig. 10a). Note that previous geobarometric data on mafic granulites were based on the mineral reactions applicable for the quartz-bearing parageneses. However, most mafic granulite xenoliths are either quartz-free or contain less than 1 vol% of quartz suggesting that granulite minerals did not coexist with quartz. Thus, we suggest that caution is necessary when applying the garnet-plagioclase-clinopyroxene-quartz (Newton and Perkins, 1982) and the clinopyroxene-plagioclase-quartz (Holland, 1983) geobarometers for mafic granulites. A scattering of P-T estimates shown in Fig. 10a could also arise from unaccounted Fe^{3+} content in Fe-Mg minerals from mafic granulite xenoliths of the Udachnaya pipe.

Although P-T conditions during the metamorphism of the studied mafic granulites correspond to amphibolite instead of granulite-facies conditions (Fig. 10), according to the classification of metamorphic rocks (Fettes et al., 2007) this inconsistency does not affect the term "granulite", which is related to the mineral paragenesis of the high-grade rock. Preservation of the granulitic parageneses beyond the granulite facies conditions is definitely due to a lack or a deficit of the fluid during their formation (Austrheim, 1987); otherwise, the granulite would be totally transformed into amphibolite.

The pressure of about 1 GPa inferred from the phase equilibria modeling indicates that the final equilibration of the studied rocks occurred at about 30 km depth, corresponding to a middle level in the 45-km-thick crust of the Siberian craton beneath the Udachnaya kimberlite pipe (e.g. Cherepanova et al., 2013). However, the inferred depth (pressure) does not necessarily mean that the crust was as thick in the Precambrian, at the time of the formation of mafic granulites, as it is

today. Thickening of the crust by the continuous underplating of new portions of mafic magmas at the crust-mantle boundary makes earlier intrusions more distant from the Moho. According to this mechanism, some lower crustal granulites could become middle crustal rocks without any vertical motion.

6.5. Interpretation of the inferred P-T conditions

Mineral assemblages of the studied granulites provide a very limited record of the early metamorphic conditions. Lamellae of orthopyroxene (and, possibly, inverted pigeonite) and ilmenite in the cores of matrix clinopyroxenes (Fig. 4 a, f) were likely formed at the onset of this stage, although the temperature of their formation cannot be reconstructed by microprobe analyses due to the tiny size of the lamellae. Ilmenite-magnetite grains indicate the highest temperatures (850–990 °C) reported for the crustal xenoliths of the Udachnaya pipe (Fig. 10a). Although no constraints on pressure at this stage are possible, it can be assumed that mafic rocks resided at the same depth in the crust due to stabilization of the Markha terrane since the late Archean (e.g. Rosen et al., 2006). P-T parameters of ~600–650 °C at 0.8 – 1.0 GPa, inferred from phase equilibrium modeling (Table 2) could be interpreted as recording the Devonian conductive paleogeotherm by the granulites trapped by kimberlitic melts. In this case, the P-T parameters of the granulites should correspond to the conductive geotherms' 35–40 mW/m^2 inferred from peridotite xenoliths from the Udachnaya pipe (e.g. Goncharov et al., 2012). However, extension of these geotherms to the lower crust (~1 GPa) gives temperatures < 400 °C, i.e. much colder conditions than those recorded by the granulites (Fig. 10a). Assuming that the real temperature of the granulites in the Devonian corresponded to the conductive geotherm, the reconstructed temperatures likely record kinetic-controlled termination of mineral reactions (so-called closure temperatures) in the rocks under fluid-deficient conditions (i.e. Rudnick, 1992).

6.6. Thermal-tectonic scenario

There is currently a consensus that the Archean mafic lower crust and subcratonic lithospheric mantle of the Siberian craton experienced a Paleoproterozoic reworking and rejuvenation (Moyen et al., 2017; Shatsky et al., 2018). This event is usually considered in light of the "vertical" tectonic processes related to deep mantle plumes (e.g. Shatsky et al., 2019) or delamination of the dense lower crust with initiation of mantle upwelling (Moyen et al., 2017). However, the following scenario of juvenile crust formation during the Precambrian collision may also deserve attention.

According to the paleotectonic reconstructions (Rosen, 2003), the Siberian craton consists of several Archean terranes (microcontinents) of independent provenance (Fig. 1). They were assembled during the Paleoproterozoic (1.8–1.9 Ga) collision, and reconstructed based on structural, geochronologic, and petrologic data on suture zones at the terrane junctions (Fig. 1). The timing of the collision was derived from the ages of granitoids in suture zones (Rosen, 2003). Interestingly, basaltic melts derived from the mantle and located apart from the collision zone have the same ages as the granitoids (Fig. 1, inset). Simultaneous formation of granitoids and basic igneous rocks might be considered as evidence of the Precambrian style of collision between different terranes via the mechanism elaborated using petrologic thermo-mechanical modeling (Perchuk et al., 2018). According to the model, convergence between two continental terranes at elevated mantle temperatures produces long-lived thick orogeny with very high Moho temperatures (up to 1100 °C). The orogeny is driven by peeling off the incoming lithospheric mantle with attached mafic lower crust and invasion of the hot partially molten asthenospheric wedge under the accreted crust. The ascending asthenosphere produces voluminous basaltic underplates (juvenile crust), which acts as a heat source for formation of granitoids and for building the lower crust via

transformation into granulites.

Bulk compositions of the studied granulites as well as of those studied by Koreshkova et al. (2009, 2011) show relatively low Mg-number (0.27–0.47, Table 2) indicating that the parent igneous rocks were likely crystallized from a highly differentiated/fractionated basic magma. During cooling in the middle/lower crust, the gabbroic rocks were transformed into mafic granulites under fluid deficient, amphibolite facies conditions. Fragments of the rocks were transported to the surface by Devonian kimberlite pipes. Therefore, these rocks resided in the crust for more than 1.4 Ga, but did not record the P-T conditions of the continental geotherm due to the blocking of mineral reactions at temperatures around 600–650 °C.

7. Conclusions

Results of our study demonstrate that thickening of the crust by the crystallization of mafic magmas occured not only as underplates at the crust-mantle boundary but also as intrusions in the middle/lower crust that were transformed into mafic granulites during continuous (more than one billion years) residence in the crust. The studied samples indicate that the dry mantle and the middle/lower crust did not provide a sufficient amount of fluids and, thus, metamorphism was predominantly fluid-deficient, while f_{O2} was controlled intrinsically by reactions involving Fe-Ti oxides and rock-forming silicate minerals. Fluid deficiency extended the stability of mafic granulites, even down to the P-T conditions of the amphibolite facies. Kinetics seemed to prevent further compositional re-equilibration of the rock minerals at temperatures corresponding to the conductive geotherm of the Siberian craton.

Declaration of Competing Interest

The authors declare that they have no known competing financial interests or personal relationships that could have appeared to influence the work reported in this paper.

Acknowledgements

Appendix A. Supplementary data

Supplementary data to this article can be found online at https://doi.org/10.1016/j.precamres.2021.106122.

References

Agashev, A.M., Ionov, D.A., Pokhilenko, N.P., Golovin, A.V., Cherepanova, Y., Sharygin, I.S., 2013. Metasomatism in lithospheric mantle roots: constraints from whole-rock and mineral chemical composition of deformed peridotite xenoliths from kimberlite pipe Udachnaya. Lithos 160, 201–215. https://doi.org/10.1016/j.lithos.2012.11.014.

Ai, Y., 1994. A revision of the garnet-clinopyroxene Fe 2+-Mg exchange geothermometer. Contrib. Miner. Petrol. 115 (4), 467–473. https://doi.org/10.1007/BF00320979.

Anderson, A.T., Lindsley, D.H., 1985. Model for the Ti magnetite or ilmenite geothermometers and oxygen barometers. Trans. Geophysical Union 66, 416.

Anderson, A.T., Wright, T.L., 1972. Phenocrysts and glass inclusions and their bearing on oxidation and mixing of basaltic magmas, Kilauea volcano, Hawaii. Am. Mineral. 57 (1–2), 188–216.

Anhaeusser, C.R., 1975. Precambrian tectonic environments. Annu. Rev. Earth Planet. Sci. 3 (1), 31–53.

Aranovich, L.Y., Newton, R.C., 1997. H2O activity in concentrated KCl and KCl-NaCl solutions at high temperatures and pressures measured by the brucite-periclase equilibrium. Contrib. Miner. Petrol. 127 (3), 261–271. https://doi.org/10.1007/s004100050279.

Arndt, N.T., 2013. The formation and evolution of the continental crust. Geochem. Perspect. 2 (3), 405.

Ashworth, J.R., Sheplev, V.S., Bryxina, N.A., Kolobov, V.Y., Reverdatto, V.V., 1998. Diffusion-controlled corona reaction and overstepping of equilibrium in a garnet granulite, Yenisey Ridge, Siberia. J. Metamorphic Geol. 16 (2), 231–246. https://doi.org/10.1111/j.1525-1314.1998.00134.x.

Austrheim, H., 1987. Eclogitization of lower crustal granulites by fluid migration through shear zones. Earth Planet. Sci. Lett. 81, 221–232. https://doi.org/10.1016/0012-821X(87)90158-0.

Berg, J.H., 1977. Dry granulite mineral assemblages in the contact aureoles of the Nain Complex, Labrador. Contrib. Mineral. Petrol. 64 (1), 33–52. https://doi.org/10.1007/BF00375284.

Bohlen, S.R., Essene, E.J., 1977. Feldspar and oxide thermometry of granulites in the Adirondack Highlands. Contrib. Miner. Petrol. 62 (2), 153–169. https://doi.org/10.1007/BF00372874.

Bohlen, S.R., Mezger, K., 1989. Origin of granulite terranes and the formation of the lowermost continental crust. Science 244 (4902), 326–329. https://doi.org/10.1126/science.244.4902.326.

Boyd, F.R., Pokhilenko, N.P., Pearson, D.G., Mertzman, S.A., Sobolev, N.V., Finger, L.W., 1997. Composition of the Siberian cratonic mantle: evidence from Udachnaya peridotite xenoliths. Contrib. Miner. Petrol. 128 (2–3), 228–246. https://doi.org/10.1007/s004100050305.

Brandelik, A., 2009. CALCMIN–an EXCEL™ Visual Basic application for calculating mineral structural formulae from electron microprobe analyses. Comput. Geosci. 35 (7), 1540–1551. https://doi.org/10.1016/j.cageo.2008.09.011.

Brown, M., Johnson, T., 2018. Secular change in metamorphism and the onset of global plate tectonics. Am. Mineral. 103 (2), 181–196. https://doi.org/10.2138/am-2018-6166.

Campanaro, B.P., Jenkins, D.M., 2017. An experimental study of chlorine incorporation in amphibole synthesized along the pargasite–ferro-pargasite join. Canad. Mineral. 55 (3), 419–436. https://doi.org/10.3749/canmin.1600082.

Carmichael, I.S., 1991. The redox states of basic and silicic magmas: a reflection of their source regions? Contrib. Miner. Petrol. 106 (2), 129–141. https://doi.org/10.1007/BF00306429.

Carmichael, I.S., Ghiorso, M.S., 1986. Oxidation-reduction relations in basic magma: a case for homogeneous equilibria. Earth Planet. Sci. Lett. 78 (2–3), 200–210. https://doi.org/10.1016/0012-821X(86)90061-0.

Cawood, P.A., Hawkesworth, C.J., Dhuime, B., 2013. The continental record and the generation of continental crust. Bulletin 125 (1–2), 14–32. https://doi.org/10.1130/B30722.1.

Cherepanova, Y., Artemieva, I.M., Thybo, H., Chemia, Z., 2013. Crustal structure of the Siberian craton and the West Siberian basin: an appraisal of existing seismic data. Tectonophysics 609, 154–183. https://doi.org/10.1016/j.tecto.2013.05.004.

Condie, K. C., Abbott, D. H., 1999. Oceanic plateaus and hotspot islands: identification and role in continental growth.

Connolly, J.A.D., Cesare, B., 1993. C-O-H-S fluid composition and oxygen fugacity in graphitic metapelites. J. Metamorph. Geol. 11 (3), 379–388. https://doi.org/10.1111/j.1525-1314.1993.tb00155.x.

Connolly, J.A., 2005. Computation of phase equilibria by linear programming: a tool for geodynamic modeling and its application to subduction zone decarbonation. Earth Planet. Sci. Lett. 236 (1–2), 524–541. https://doi.org/10.1016/j.epsl.2005.04.033.

Dawson, J.B., Smith, J.V., 1987. Reduced sapphirine granulite xenoliths from the Lace Kimberlite, South Africa; implications for the deep structure of the Kaapvaal Craton. Contrib. Miner. Petrol. 95 (3), 376–383. https://doi.org/10.1007/BF00371851.

Doucet, L.S., Peslier, A.H., Ionov, D.A., Brandon, A.D., Golovin, A.V., Goncharov, A.G., Ashchepkov, I.V., 2014. High water contents in the Siberian cratonic mantle linked to metasomatism: an FTIR study of Udachnaya peridotite xenoliths. Geochim. Cosmochim. Acta 137, 159–187. https://doi.org/10.1016/j.gca.2014.04.011.

Ellis, D.J., Green, D.H., 1979. An experimental study of the effect of Ca upon garnet-clinopyroxene Fe-Mg exchange equilibria. Contrib. Miner. Petrol. 71 (1), 13–22. https://doi.org/10.1007/BF00371878.

Fedortchouk, Y., Canil, D., Carlson, J.A., 2005. Dissolution forms in Lac de Gras diamonds and their relationship to the temperature and redox state of kimberlite magma. Contrib. Miner. Petrol. 150, 54–69. https://doi.org/10.1007/s00410-005-0003-1.

Fettes, D., Desmons, J. (Ed.), 2007. Metamorphic rocks: a classification and glossary of terms: recommendations of the International Union of Geological Sciences Subcommission on the Systematics of Metamorphic Rocks. – 244 S., Cambridge 2007, Cambridge University Press.

François, C., Philippot, P., Rey, P., Rubatto, D., 2014. Burial and exhumation during Archean sagduction in the East Pilbara granite-greenstone terrane. Earth Planet. Sci. Lett. 396, 235–251. https://doi.org/10.1016/j.epsl.2014.04.025.

Fuhrman, M.L., Lindsley, D.H., 1988. Ternary-feldspar modeling and thermometry. American mineralogist 73 (3–4), 201–215.

Gao, S., Rudnick, R. L., Yuan, H. L., Liu, X. M., Liu, Y. S., Xu, W. L., Ling, W.L., Ayers Jh., Wang C.H. Wang, Q. H., 2004. Recycling lower continental crust in the North China craton. Nature, 432(7019), 892-897. 10.1038/nature03162.

Goncharov, A.G., Ionov, D.A., 2012. Redox state of deep off-craton lithospheric mantle: new data from garnet and spinel peridotites from Vitim, southern Siberia. Contrib. Miner. Petrol. 164 (5), 731–745.

Goncharov, A.G., Ionov, D.A., Doucet, L.S., Pokhilenko, L.N., 2012. Thermal state, oxygen fugacity and COH fluid speciation in cratonic lithospheric mantle: new data on peridotite xenoliths from the Udachnaya kimberlite, Siberia. Earth Planet. Sci. Lett. 357, 99–110. https://doi.org/10.1016/j.epsl.2012.09.016.

Green, E.C.R., White, R.W., Diener, J.F.A., Powell, R., Holland, T.J.B., Palin, R.M., 2016. Activity–composition relations for the calculation of partial melting equilibria in metabasic rocks. J. Metamorph. Geol. 34 (9), 845–869. https://doi.org/10.1111/jmg.12211.

Griffin, W.L., Heier, K.S., 1973. Petrological implications of some corona structures. Lithos 6 (4), 315–335. https://doi.org/10.1016/0024-4937(73)90051-0.

Griffin, W.L., O'Reilly, S.Y, Abe, N. Aulbach, S., Davies, R.M., Pearson, N.J., Doyle, B.J., Kivi, K., 2003. The origin and evolution of Archean lithospheric mantle. Precambrian Res. 127, 19–41.

Hammerli, J., Kemp, A. I., Barrett, N., Wing, B. A., Roberts, M., Arculus, R. J., Pierre B., Nude P.M. Rankenburg, K., 2017. Sulfur isotope signatures in the lower crust: a SIMS study on S-rich scapolite of granulites. Chemical Geology, 454, 54-66. 10.1016/j.chemgeo.2017.02.016.

Hammond, P.A., Taylor, L.A., 1982. The ilmenite titano-magnetite assemblage-kinetics of reequilibration. Earth Planet. Sci. Lett. 61, 143–150.

Harley, S.L., 1984. An experimental study of the partitioning of Fe and Mg between garnet and orthopyroxene. Contrib. Miner. Petrol. 86 (4), 359–373. https://doi.org/10.1007/BF01187140.

Harlov, D.E., 1992. Comparative oxygen barometry in granulites, Bamble Sector. SE Norway. The Journal of Geology 100 (4), 447–464.

Harlov, D.E., 2000. Titaniferous magnetite–ilmenite thermometry and titaniferous magnetite–ilmenite–orthopyroxene–quartz oxygen barometry in granulite facies gneisses, Bamble Sector, SE Norway: implications for the role of high-grade CO_2-rich fluids during granulite genesis. Contrib. Miner. Petrol. 139 (2), 180–197. https://doi.org/10.1007/PL00007670.

Holland, T.J.B., 1983. The experimental determination of activities in disordered and short-range ordered jadeitic pyroxenes. Contrib. Miner. Petrol. 82 (2–3), 214–220. https://doi.org/10.1007/BF01166616.

Holland, T., Powell, R., 1996. Thermodynamics of order-disorder in minerals; II, Symmetric formalism applied to solid solutions. Am. Mineral. 81 (11–12), 1425–1437. https://doi.org/10.2138/am-1996-11-1215.

Holland, T.J.B., Powell, R.T.J.B., 1998. An internally consistent thermodynamic data set for phases of petrological interest. J. Metamorph. Geol. 16 (3), 309–343. https://doi.org/10.1111/j.1525-1314.1998.00140.x.

Ionov, D.A., Doucet, L.S., Carlson, R.W., Golovin, A.V., Korsakov, A.V., 2015. Post-Archean formation of the lithospheric mantle in the central Siberian craton: Re–Os and PGE study of peridotite xenoliths from the Udachnaya kimberlite. Geochim. Cosmochim. Acta 165, 466–483.

Jenkins, D.M., 2019. The incorporation of chlorine into calcium amphibole. Am. Mineral. 104 (4), 514–524. https://doi.org/10.2138/am-2019-6768.

Jennings, E.S., Holland, T.J., 2015. A simple thermodynamic model for melting of peridotite in the system NCFMASOCr. J. Petrol. 56 (5), 869–892. https://doi.org/10.1093/petrology/egv020.

Johnson, T.E., Brown, M., Goodenough, K.M., Clark, C., Kinny, P.D., White, R.W., 2016. Subduction or sagduction? ambiguity in constraining the origin of ultramaficmafic bodies in the Archean crust of NW Scotland. Precambr. Res. 283, 89–105.

Kamenetsky, V.S., Kamenetsky, M.B., Sharygin, V.V., Faure, K., Golovin, A.V., 2007. Chloride and carbonate immiscible liquids at the closure of the kimberlite magma evolution (Udachnaya-East kimberlite, Siberia). Chem. Geol. 237 (3–4), 384–400. https://doi.org/10.1016/j.chemgeo.2006.07.010.

Keller, L.M., Wirth, R., Rhede, D., Kunze, K., Abart, R., 2008. Asymmetrically zoned reaction rims: assessment of grain boundary diffusivities and growth rates related to natural diffusion-controlled mineral reactions. J. Metamorph. Geol. 26 (1), 99–120. https://doi.org/10.1111/j.1525-1314.2007.00747.x.

Kelley, K.A., Cottrell, E., 2012. The influence of magmatic differentiation on the oxidation state of Fe in a basaltic arc magma. Earth Planet. Sci. Lett. 329, 109–121. https://doi.org/10.1016/j.epsl.2012.02.010.

Kinny, P.D., Griffin, B., Heaman, L.M., Brakhfogel, F.F., Spetsius, Z.V., 1997. SHRIMP U-Pb ages of perovskite from Yakutian kimberlites. Geol Geofiz 38, 91–99.

Koreshkova, M.Y., Downes, H., Nikitina, L.P., Vladykin, N.V., Larionov, A.N., Sergeev, S.A., 2009. Trace element and age characteristics of zircons in granulite xenoliths from the Udachnaya kimberlite pipe, Siberia. Precambr. Res. 168 (3–4), 197–212. https://doi.org/10.1016/j.precamres.2008.09.007.

Koreshkova, M.Y., Downes, H., Levsky, L.K., Vladykin, N.V., 2011. Petrology and geochemistry of granulite xenoliths from Udachnaya and Komsomolskaya kimberlite pipes, Siberia. J. Petrol. 52 (10), 1857–1885. https://doi.org/10.1093/petrology/egr033.

Kunz, B.E., White, R.W., 2019. Phase equilibrium modelling of the amphibolite to granulite facies transition in metabasic rocks (Ivrea Zone, NW Italy). J. Metamorph. Geol. 37 (7), 935–950. https://doi.org/10.1111/jmg.12478.

Lamb, W., Valley, J.W., 1984. Metamorphism of reduced granulites in low-CO_2 vapour-free environment. Nature 312 (5989), 56–58. https://doi.org/10.1038/312056a0.

Leake, B.E., Woolley, A.R., Arps, C.E., Birch, W.D., Gilbert, M.C., Grice, J.D., Linthout, K., 1997. Nomenclature of amphiboles: report of the Subcommittee on Amphiboles of the International Mineralogical Association Commission on new minerals and mineral names. Mineral. Mag. 61 (405), 295–310.

Lepage, L.D., 2003. ILMAT: an Excel worksheet for ilmenite-magnetite geothermometry and geobarometry. Comput. Geosci. 29 (5), 673–678.

Lindsley, D.H., 1983. Pyroxene thermometry. Am. Mineral. 68 (5–6), 477–493.

Liu, Y., Taylor, L.A., Sarbadhikari, A.B., Valley, J.W., Ushikubo, T., Spicuzza, M.J., Sobolev, N.V., 2009. Metasomatic origin of diamonds in the world's largest diamondiferous eclogite. Lithos 112, 1014–1024. https://doi.org/10.1016/j.lithos.2009.06.036.

Manning, C.E., Aranovich, L.Y., 2014. Brines at high pressure and temperature: thermodynamic, petrologic and geochemical effects. Precambr. Res. 253, 6–16. https://doi.org/10.1016/j.precamres.2014.06.025.

McLelland, J.M., Whitney, P.R., 1980. Compositional controls on spinel clouding and garnet formation in plagioclase of olivine metagabbros, Adirondack Mountains, New York. Contrib. Miner. Petrol. 73 (3), 243–251. https://doi.org/10.1007/BF00381443.

Moecher, D.P., Essene, E.J., Anovitz, L.M., 1988. Calculation and application of clinopyroxene-garnet-plagioclase-quartz geobarometers. Contrib. Miner. Petrol. 100 (1), 92–106. https://doi.org/10.1007/BF00399441.

Morimoto, N., 1988. Nomenclature of pyroxenes. Mineral. Petrol. 39 (1), 55–76. https://doi.org/10.1007/BF01226262.

Moyen, J.F., Martin, H., 2012. Forty years of TTG research. Lithos 148, 312–336. https://doi.org/10.1016/j.lithos.2012.06.010.

Moyen, J.-F., Paquette, J.L., Ionov, D.A., Gannoun, A., Korsakov, A.V., Golovin, A.V., Moine, B.N., 2017. Paleoproterozoic rejuvenation and replacement of Archaean lithosphere: evidence from zircon U-Pb dating and Hf isotopes in crustal xenoliths at Udachnaya, Siberian craton. Earth Planet. Sci. Lett. 457, 149–159. https://doi.org/10.1016/j.epsl.2016.09.046.

Müller, T., Dohmen, R., Becker, H.W., Ter Heege, J.H., Chakraborty, S., 2013. Fe–Mg interdiffusion rates in clinopyroxene: experimental data and implications for Fe–Mg exchange geothermometers. Contrib. Miner. Petrol. 166 (6), 1563–1576. https://doi.org/10.1007/s00410-013-0941-y.

Newton, R.C., Perkins, D.I.I.I., 1982. Thermodynamic calibration of geobarometers based on the assemblages garnet-plagioclase-orthopyroxene (clinopyroxene)-quartz. Am. Mineral. 67 (3–4), 203–222.

Pearson, N.J., O'Reilly, S.Y., Griffin, W.L., 1995. The crust-mantle boundary beneath cratons and craton margins: a transect across the south-west margin of the Kaapvaal craton. Lithos 36 (3–4), 257–287. https://doi.org/10.1016/0024-4937(95)00021-6.

Perchuk, A.L., Burchard, M., Schertl, H.P., Maresch, W.V., Gerya, T.V., Bernhardt, H.J., Vidal, O., 2009. Diffusion of divalent cations in garnet: multi-couple experiments. Contrib. Miner. Petrol. 157 (5), 573. https://doi.org/10.1007/s00410-008-0353-6.

Perchuk, A.L., Morgunova, A.A., 2014. Variable P-T paths and HP-UHP metamorphism in a Precambrian terrane, Gridino, Russia: petrological evidence and geodynamic implications. Gondwana Res. 25 (2), 614–629. https://doi.org/10.1016/j.gr.2012.09.009.

Perchuk, A.L., Safonov, O.G., Smit, C.A., van Reenen, D.D., Zakharov, V.S., Gerya, T.V., 2018. Precambrian ultra-hot orogenic factory: making and reworking of continental crust. Tectonophysics 746, 572–586. https://doi.org/10.1016/j.tecto.2016.11.041.

Perchuk, L.L., Gerya, T.V., van Reenen, D.D., Kramers, J.D., McCourt, S., 2011. Formation and evolution of Precambrian granulite terranes: a gravitational redistribution model. Geol. Soc. Am. Memoirs 207, 289–310. https://doi.org/10.1130/2011.1207(15).

Pisarevsky, S.A., Natapov, L.M., Donskaya, T.V., Gladkochub, D.P., Vernikovsky, V.A., 2008. Proterozoic Siberia: a promontory of Rodinia. Precambr. Res. 160 (1–2), 66–76. https://doi.org/10.1016/j.precamres.2007.04.016.

Powell, R., 1985. Regression diagnostics and robust regression in geothermometer/geobarometer calibration: the garnet-clinopyroxene geothermometer revisited. J. Metamorph. Geol. 3 (3), 231–243. https://doi.org/10.1111/j.1525-1314.1985.tb00319.x.

Powell, R., Holland, T.J.B.H., Worley, B., 1998. Calculating phase diagrams involving solid solutions via non-linear equations, with examples using THERMOCALC. J. Metamorph. Geol. 16 (4), 577–588. https://doi.org/10.1111/j.1525-1314.1998.00157.x.

Ravna, K., 2000. The garnet–clinopyroxene Fe2+–Mg geothermometer: an updated calibration. J. Metamorph. Geol. 18 (2), 211–219. https://doi.org/10.1046/j.1525-1314.2000.00247.x.

Redhummer, G.J., Amthauer, G., Lottermoser, W., Treutmann, W., 2000. Synthesis and structural properties of clinopyroxenes of the hedenbergite $CaFe^{2+}Si_2O_6$–aegirine $NaFe^{3+}Si_2O_6$ solid-solution series. Eur. J. Mineral. 12 (1), 105–120. https://doi.org/10.1127/0935-1221/2000/0012-0105.

Rozel, A.B., Golabek, G.J., Jain, C., Tackley, P.J., Gerya, T., 2017. Continental crust formation on early Earth controlled by intrusive magmatism. Nature 545, 332–335. https://doi.org/10.1038/nature22042.

Rosen, O.M., Condie, K.C., Natapov, L.M., Nozhkin, A.D., 1994. Archean and Early Proterozoic evolution of the Siberian craton: a preliminary assessment. Develop. Precambr. Geol. 11, 411–459. https://doi.org/10.1016/S0166-2635(08)70228-7.

Rosen, O.M., 2003. The Siberian craton: tectonic zonation and stages of evolution. Geotectonics 37 (3), 175–192.

Rosen, O.M., Levsky, L.K., Zhuravlev, D.Z., Rotman, A.Ya., Spetsius, Z.V., Makeev, A.F., Zinchuk, N.N., Manakov, A.V., Serenko, V.P., 2006. Palaeoproterozoic accretion in the northeast Siberian craton: isotopic dating of the Anabar collision system. Stratigr. Geol. Correl. 14, 581–601. https://doi.org/10.1134/S0869593806060013.

Rudnick, R.L., 1992. Xenoliths—samples of the lower continental crust. Continental lower crust 23, 269–316.

Rudnick, R.L., 1995. Making continental crust. Nature 378 (6557), 571–578. https://doi.org/10.1038/378571a0.

Rudnick, R.L., Fountain, D.M., 1995. Nature and composition of the continental crust: a lower crustal perspective. Rev. Geophys. 33 (3), 267–309. https://doi.org/10.1029/95RG01302.

Schumacher, J.C., 1997. Appendix 2: the estimation of ferric iron in electron microprobe analysis of amphiboles. Mineral. Mag. 61 (405), 312–321. https://doi.org/10.1017/S0026461X00011397.

Skippen, G.B., Marshall, D.D., 1991. The metamorphism of granulites and devolatilization of the lithosphere. Canad. Mineral. 29 (4), 693–705.

Shatsky, V. S., Rudnick, R. L., Jagoutz, E., 1990. Mafic granulites from Udachnaya pipe, Yakutia: samples of Archaean lower crust. Deep seated magmatism and evolution of the lithosphere of Siberian Platform. Novosibirsk: Siberian Branch of the USSR Academy of Sciences, 45-46.

Shatsky, V.S., Buzlukova, L.V., Jagoutz, E., Koz'menko, O.A., Mityukhin, S.I., 2005. Structure and evolution of the lower crust of the Daldyn-Alakit district in the Yakutian Diamond Province (from data on xenoliths). Russ. Geol. Geophys. 46 (12), 1252–1270.

Shatsky, V., Ragozin, A., Zedgenizov, D., Mityukhin, S., 2008. Evidence for multistage evolution in a xenolith of diamond-bearing eclogite from the Udachnaya kimberlite pipe. Lithos 105 (3–4), 289–300. https://doi.org/10.1016/j.lithos.2008.04.008.

Shatsky, V.S., Malkovets, V.G., Belousova, E.A., Tretiakova, I.G., Griffin, W.L., Ragozin, A.L., O'Reilly, S.Y., 2016. Tectonothermal evolution of the continental crust beneath the Yakutian diamondiferous province (Siberian craton): U-Pb and Hf isotopic evidence on zircons from crustal xenoliths of kimberlite pipes. Precambr. Res. 282, 1–20. https://doi.org/10.1016/j.precamres.2016.06.022.

Shatsky, V.S., Malkovets, V.G., Belousova, E.A., Tretiakova, I.G., Griffin, W.L., Ragozin, A.L., O'Reilly, S.Y., 2018. Multi-stage modification of Paleoarchean crust beneath the Anabar tectonic province (Siberian craton). Precambr. Res. 305, 125–144. https://doi.org/10.1016/j.precamres.2017.11.017.

Shatsky, V. S., Wang, Q., Skuzovatov, S. Y., Ragozin, A. L., 2019. The crust-mantle evolution of the Anabar tectonic province in the Siberian Craton: Coupled or decoupled? Precambrian Research. Vol.332. - Art.105388.

Smith, C.M., Canil, D., Rowins, S.M., Friedman, R., 2012. Reduced granitic magmas in an arc setting: the Catface porphyry Cu–Mo deposit of the Paleogene Cascade Arc. Lithos 154, 361–373. https://doi.org/10.1016/j.lithos.2012.08.001.

Suvorov, V.D., Melnik, E.A., Thybo, H., Perchuc, E., Parasotka, B.S., 2006. Seismic velocity model of the crust and uppermost mantle around the Mirnyi kimberlite Field in Siberia. Tectonophysics 420, 49–73.

Thébaud, N., Rey, P.F., 2013. Archean gravity-driven tectonics on hot and flooded continents: controls on long-lived mineralised hydrothermal systems away from continental margins. Precambr. Res. 229, 93–104. https://doi.org/10.1016/j.precamres.2012.03.001.

Tretiakova, I.G., Belousova, E.A., Malkovets, V.G., Griffin, W.L., Piazolo, S., Pearson, N. J., Nishido, H., 2017. Recurrent magmatic activity on a lithosphere-scale structure: Crystallization and deformation in kimberlitic zircons. Gondwana Res. 42, 126–132. https://doi.org/10.1016/j.gr.2016.10.006.

Török, K., Dégi, J., Szép, A., Marosi, G., 2005. Reduced carbonic fluids in mafic granulite xenoliths from the Bakony-Balaton Highland Volcanic Field, W-Hungary. Chem. Geol. 223 (1–3), 93–108. https://doi.org/10.1016/j.chemgeo.2005.05.010.

Valley, J.W., Bohlen, S.R., Essene, E.J., Lamb, W., 1990. Metamorphism in the Adirondacks: II. The role of fluids. J. Petrol. 31 (3), 555–596. https://doi.org/10.1093/petrology/31.3.555.

Van Kranendonk, M.J., 2004. Archaean tectonics 2004: a review. Precambr. Res. 131 (3–4), 143–151. https://doi.org/10.1016/j.precamres.2003.12.008.

Van Kranendonk, M.J., 2010. Two types of Archean continental crust: plume and plate tectonics on early Earth. Am. J. Sci. 310 (10), 1187–1209. https://doi.org/10.2475/10.2010.01.

Volfinger, M., Robert, J.L., Vielzeuf, D., Neiva, A.M.R., 1985. Structural control of the chlorine content of OH-bearing silicates (micas and amphiboles). Geochim. Cosmochim. Acta 49 (1), 37–48. https://doi.org/10.1016/0016-7037(85)90189-9.

Webster, J.D., Baker, D.R., Aiuppa, A., 2018. Halogens in mafic and intermediate-silica content magmas. In: The Role of Halogens in Terrestrial and Extraterrestrial Geochemical Processes. Springer, Cham, pp. 307–430. https://doi.org/10.1007/978-3-319-61667-4_6.

Whitney, D.L., Evans, B.W., 2010. Abbreviations for names of rock-forming minerals. Am. Mineral. 95 (1), 185–187. https://doi.org/10.2138/am.2010.3371.

Wood, B.J., Banno, S., 1973. Garnet-orthopyroxene and orthopyroxene-clinopyroxene relationships in simple and complex systems. Contrib. Mineral. Petrol. 42 (2), 109–124. https://doi.org/10.1007/BF00371501.

Yang, C., Wei, C., 2017. Two phases of granulite facies metamorphism during Neoarchean and Paleoproterozoic in the East Hebei, North China Craton: records from mafic granulites. Precambr. Res. 301, 49–64. https://doi.org/10.1016/j.precamres.2017.09.005.